

AD-A125 221

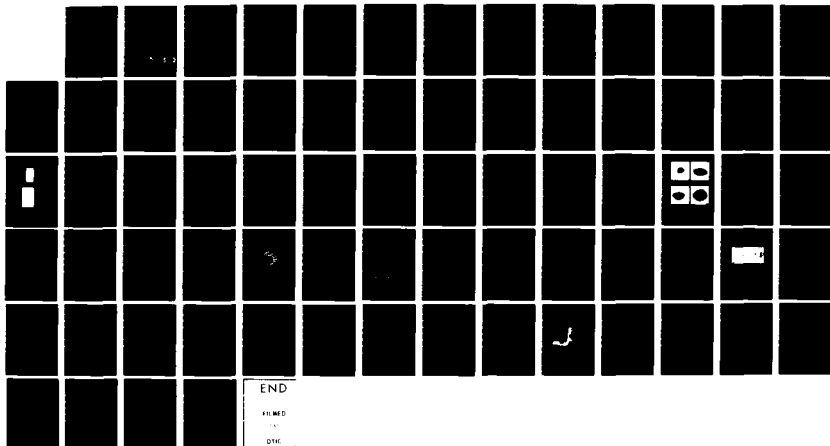
A FREE ELECTRON LASER DRIVEN BY A LONG PULSE INDUCTION
LINAC(U) NAVAL RESEARCH LAB WASHINGTON DC
C W ROBERSON ET AL. 07 MAR 83 NRL-MR-5013

1/1

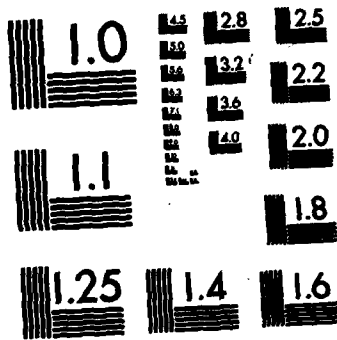
UNCLASSIFIED

F/G 17/8

NL



END
FILMED
BY
DHE



MICROCOPY RESOLUTION TEST CHART
NATIONAL BUREAU OF STANDARDS-1963-A

2

A Free Electron Laser Driven by a Long Pulse Induction Linac

C. W. ROBERSON,* J. A. PASOUR, F. MAKO,**
R. LUCEY†, AND P. SPRANGLE§

*Beam Dynamics Branch
Plasma Physics Division*

*Office of Naval Research
Arlington, VA*

***JAYCOR
Alexandria, VA*

*†Pulse Sciences Inc.
San Leandro, CA*

*§Plasma Theory Branch
Plasma Physics Division*

March 7, 1983

AD A 1 25221

DTIC FILE COPY



DTIC
ELECTE
MAR 3 1983
S D
B

NAVAL RESEARCH LABORATORY
Washington, D.C.

Approved for public release; distribution unlimited.

83 03 02 054

REPORT DOCUMENTATION PAGE		READ INSTRUCTIONS BEFORE COMPLETING FORM
1. REPORT NUMBER NRL Memorandum Report 5013	2. GOVT ACCESSION NO. <i>A125 221</i>	3. RECIPIENT'S CATALOG NUMBER
4. TITLE (and Subtitle) A FREE ELECTRON LASER DRIVEN BY A LONG PULSE INDUCTION LINAC	5. TYPE OF REPORT & PERIOD COVERED Interim report on a continuing NRL problem.	
	6. PERFORMING ORG. REPORT NUMBER	
7. AUTHOR(s) C. W. Roberson,* J. A. Pasour, F. Mako,** R. Lucey,† and P. Sprangle	8. CONTRACT OR GRANT NUMBER(s)	
9. PERFORMING ORGANIZATION NAME AND ADDRESS Naval Research Laboratory Washington, DC 20375	10. PROGRAM ELEMENT, PROJECT, TASK AREA & WORK UNIT NUMBERS 61153N; RR0110941; 47-1484-0-3	
11. CONTROLLING OFFICE NAME AND ADDRESS Office of Naval Research Arlington, VA 22217	12. REPORT DATE March 7, 1983	
	13. NUMBER OF PAGES 71	
14. MONITORING AGENCY NAME & ADDRESS (if different from Controlling Office)	15. SECURITY CLASS. (of this report) UNCLASSIFIED	
	15a. DECLASSIFICATION/DOWNGRADING SCHEDULE	
16. DISTRIBUTION STATEMENT (of this Report) Approved for public release; distribution unlimited.		
17. DISTRIBUTION STATEMENT (of the abstract entered in Block 20, if different from Report)		
18. SUPPLEMENTARY NOTES *Present address: Office of Naval Research, Arlington, VA **Present address: JAYCOR, Alexandria, VA †Present address: Pulse Sciences Inc., San Leandro, CA (Continues)		
19. KEY WORDS (Continue on reverse side if necessary and identify by block number) Free electron lasers Induction linear accelerator <i>Approved</i>		
20. ABSTRACT (Continue on reverse side if necessary and identify by block number) An overview of Free Electron Laser (FEL) research is presented, and a high-current, long pulse FEL experiment is described. The overview consists of a description of the FEL mechanism and operating regimes and a historical survey of experimental research. Preliminary results are presented from an FEL experiment using both linear and diffusive magnetic wigglers with a long pulse induction linac (800 kV, 800 A, 2 μsec). Mode identification of the ~100 kW output radiation pulse indicates that both FEL and cyclotron emission is present. <i>Approved</i>		

less than an approval

microsec

less than an approval

18. Supplementary Notes (Continued)

To be published in *Infrared and Millimeter Waves, Vol. 10*, ed. by K. J. Button, Academic Press, N.Y.

CONTENTS

I.	INTRODUCTION	1
II.	FEL MECHANISM	2
III.	FEL EXPERIMENTAL RESEARCH	5
IV.	FEL OPERATING REGIMES	12
V.	ACCELERATOR DEVELOPMENT	19
VI.	THE FEL APPARATUS	28
VII.	RADIATION MEASUREMENTS	45
VIII.	CONCLUSIONS AND FUTURE DIRECTIONS	61
	ACKNOWLEDGEMENTS	62
	REFERENCES	63



Accession For	
NTIS GRA&I	<input checked="" type="checkbox"/>
DTIC TAB	<input type="checkbox"/>
Unannounced	<input type="checkbox"/>
Justification	
By _____	
Distribution/	
Availability Codes	
Dist	Avail and/or Special
A	

A FREE ELECTRON LASER DRIVEN BY A LONG PULSE INDUCTION LINAC

I. Introduction

In the last five years, free electron laser (FEL) research has expanded rapidly. Great progress has been made both in the theoretical understanding of the mechanism and in the experimental demonstration of the validity of many features predicted by theory. The FEL has attracted this interest because of its promise as a tunable, powerful, and efficient source of radiation over a very large frequency range. The strong dependence of output frequency on electron energy ($\omega \propto \gamma^2$) makes scaling attractive. Furthermore, the availability of very high power electron beams ($\gg 1$ GW) makes possible the generation of high power radiation in regions of the spectrum where other practical high power sources do not exist.

In this paper we will present an overview of FEL research and then describe in some detail an ongoing experiment designed to produce mm-wave output from a long pulse induction linac ($\tau \approx 2 \mu\text{sec}$). In Section II we will describe the FEL mechanism, and a brief history of FEL experimental research will be presented in Section III. Section IV will describe the various FEL operating regimes and discuss the beam requirements for operation in the Raman regime. Accelerator development and diode characteristics will be discussed in Section V and the long pulse induction linac described. Our FEL experiment will be described in Section VI along with a comparison of various wigglers. The experimental results will be presented in Section VII and future directions for the experiment and conclusions in Section VIII.

Manuscript approved December 28, 1982.

II. FEL Mechanism

To understand the FEL, let us consider a very low current electron beam so that space charge forces are not important. We assume the initial velocity of the electron beam is in the axial direction and we have a simple linear wiggler in the y direction.

Let

$$\underline{v}_b = v_b \hat{z} \quad (1)$$

and

$$\underline{B}_w = B_w \sin(k_w z) \hat{y} . \quad (2)$$

Then

$$\underline{v}_w = v_w \cos(k_w z) \hat{x} . \quad (3)$$

Here, v_b is the beam velocity, B_w the wiggler magnetic field, and v_w is the wiggle velocity that results from the Lorentz force acting on the particle as it passes through the wiggler field. We now assume the presence of a linearly polarized radiation field

$$\underline{E} + \underline{B} = E \cos(kz - \omega t) \hat{x} + B \sin(kz - \omega t) \hat{y} \quad (4)$$

This radiation field will exist as part of the noise spectrum in the case of the oscillator, or will be supplied externally in the case of an amplifier.

As a result of the wiggler and the radiation field, a pondermotive force in the z direction develops

$$\underline{F} = \frac{q}{c} (\underline{v}_w \times \underline{B} + \underline{v} \times \underline{B}_w) \hat{z} \propto \sin[(k + k_w) z - \omega t] \hat{z} \quad (5)$$

This force arises from the interaction between v_w and the magnetic component of the radiation field and from the perturbed velocity \underline{v} (which results from $\underline{v}_b \times \underline{B}$) interacting with the wiggler field.

This pondermotive force drives a current, δJ_z . From the continuity equation $q \partial \delta n / \partial t = \nabla \cdot \delta \underline{J}$, we obtain a density modulation of the form

$$\delta n \propto \cos [(k + k_w) z - \omega t]. \quad (6)$$

This density modulation of the electron beam, driven by the pondermotive force, results in a current which can cause radiation in phase with the radiation field:

$$\underline{\delta J} = q \delta n \underline{v}_w \propto \cos (kz - \omega t) \hat{x}. \quad (7)$$

Therefore the pondermotive force causes the beam to bunch and the electrons to radiate coherently and in phase with the existing radiation. Thus the original radiation grows, which increases δn , increasing δJ and so on until saturation occurs.

If $\delta n((k + k_w), \omega)$ is at a frequency and wave number that is also a beam mode, then we have a collective free electron laser. Then to determine the wavelength scaling, we assume the phase velocity of the pondermotive wave is near the beam velocity

$$v_{ph} = \frac{\omega}{k+k_w} = v_b \quad (8)$$

Then using $\omega = ck$, we obtain

$$\lambda = \frac{1-\beta}{\beta} \lambda_w = \frac{\lambda_w}{2\gamma^2} \quad (9)$$

This is the wavelength scaling law that is such an important feature of the FEL. If the beam current is high, the pondermotive force will drive a collective space charge wave. This enhances the interaction and increases the intrinsic efficiency. However the higher current introduces an additional complication, that of the beam rapidly expanding due to its own space charge. The simplest configuration to confine the beam is an axial magnetic field. This introduces the cyclotron modes on the beam, which can result in competing interactions.

III. FEL Experimental Research

As is typical in a rapidly developing, complex field such as free electron lasers, experiments have lagged behind theory to a large degree. In the last 2-3 years, however, scores of experiments have been proposed and undertaken to explore the many aspects of FEL operation predicted by theory. Although only preliminary results have been reported from most of these experiments, indications are that the FEL mechanism is a viable, tunable source of radiation from millimeter waves to the infrared. Experiments now underway are attempting to extend the range of operation into the visible and even beyond.

Free electron laser experiments have evolved along two distinct paths depending on the type of electron accelerator used. High current, relatively low particle energy electron beams typically from Marx type generators have been used for FEL experiments in the collective regime. More conventional accelerators such as RF linacs, which produce much higher energy electrons but at much lower current levels, have proved useful for FEL research in the Compton or single particle regime. Madey and coworkers¹ at Stanford have pioneered the Compton regime research using a superconducting linac together with a helical magnetic wiggler field (Elias et al., 1976; Deacon et al., 1977). They initially performed amplifier experiments at $\lambda = 10.6 \mu\text{m}$ and later demonstrated laser oscillator operation at $\lambda = 3.4 \mu\text{m}$ using a 43 MeV beam having a peak micropulse current of 2.6 A. The efficiency (laser energy/beam energy) of the oscillator was less than 10^{-4} , but it was suggested that a much higher efficiency could be achieved by providing for multiple passes of the electron beam through the FEL interaction region. However, the increasing beam energy spread with each pass becomes a limiting factor.

More recently, the Stanford group has collaborated with LURE on an experiment using the ACO storage ring in Orsay, France (Bazin et al., 1982). In this experiment a superconducting undulator ($B_{\perp} = 4$ kG, $L \sim 1$ m) was placed on a straight section of the storage ring, which was typically operated at 150 MeV with a bunch current of ~ 10 mA. An argon laser ($\lambda = 4880$ Å or 5145 Å) having a power density of ~ 1.6 kW/cm² was amplified in the interaction region. The maximum gain reported was $\sim 4 \times 10^{-4}$ per pass, hence oscillator experiments would be extremely difficult with the original apparatus. Consequently, the group is attempting to increase the gain by substituting an optical klystron for the undulator.

Somewhat similar experiments are underway at Frascati using the Adone storage ring (Barbini and Vignola, 1982) and at Brookhaven using the VUV storage ring (Luccio, 1982). Another storage ring FEL experiment has been proposed for BESSY in Berlin (Gaupp, 1982).

Another set of similar experiments employing rf linacs in conjunction with CO₂ lasers and planar, permanent magnet wigglers have recently been undertaken. These experiments were initiated at Los Alamos, TRW, and Math Sciences Northwest. The permanent magnet wigglers used in these experiments are convenient for studying variable wiggler efficiency enhancement schemes by changing either the wiggler period or amplitude with axial distance. In initial experiments, the groups have concentrated on measuring the energy loss of the electrons passing through the interaction region, because the gains or efficiencies are so low that it is very difficult to accurately measure the amplified output signal in the presence of the large input laser signal (20 - 1000 MW).

Based on measurements of electron energy loss, the TRW group has calculated an efficiency of 0.07% and a gain of 2.7% using a wiggler with an amplitude taper of 2.25% (Boehmer et. al., 1982). This efficiency is an order of magnitude higher than the theoretical value with no taper. By using a more powerful laser than the TRW group (1 GW vs 2 MW) the Los Alamos group can achieve high efficiency (~ 2%) but lower gain (Warren et. al., 1982). (Note that the input laser power is not included in the efficiency calculation). The Los Alamos experiment is now being converted to an oscillator mode.

Additional low-current-regime experiments are being performed using microtron accelerators at Bell Labs (Shaw and Patel, 1982) and at Frascati (Bizzarri et al., 1982). These accelerators operate at up to ~20 MeV with peak current of ~ 5 A, and the Frascati microtron is being upgraded to > 30 MeV. Bell Labs is using a 10 m long helical wiggler with a 20 cm period to generate 100 - 400 μm radiation by tuning the beam energy from 10-20 MeV. Frascati uses a 2.25 m long permanent magnet wiggler with a period of 5 cm for output at ~ 15-20 μm .

A different, but quite interesting approach is being pursued at the University of California - Santa Barbara (Elias and Ramian, 1982). The UCSB group is using a recirculating electrostatic accelerator to achieve high average power, good beam quality, and high overall FEL efficiency. If all the beam could be recovered, the device could essentially operate dc. The group hopes to use the 2A, 3 MeV electron beam to generate FIR to submillimeter radiation in a single stage FEL, and then to perform a two stage experiment to generate visible to IR output.

High current, relatively low particle energy FEL experiments have achieved impressively high gains and radiation power levels at much lower frequencies than the high particle energy experiments. However, these experiments are characterized by a different set of problems. High current beams are typically produced by Marx-type generators and in general have higher energy spreads than low current beams. Self field effects become important in the propagation of these beams, and the axial magnetic field required to confine the beam can result in large amounts of cyclotron type emission.

The first operation of a device employing what we now call the FEL mechanism was reported over 20 years ago by Phillips (1960). He called the device a Ubitron and built several microwave tube-type versions which behaved impressively in S-band ($\sim 2-3$ GHz). The wiggler typically consisted of alternately wound co-axial coils and the interaction length was ~ 50 cm. Peak microwave output power in excess of 1 MW was achieved using a beam of ~ 150 kV and < 100 A, corresponding to an efficiency of $\sim 10\%$. Scaling this device into the mm wavelength range was restricted at the time because of the limited voltage of available electron guns. However, the introduction of high current, higher voltage Marx type generators made possible a renewed effort in the generation of high power mm waves using this mechanism.

High current (> 1 kA) FEL experiments were originally referred to as stimulated scattering, and their origins can be traced to early experiments at Cornell University and the Naval Research Lab in which large radiated powers were observed when an intense beam was modulated by a slow wave structure or a rippled magnetic field (Nation, 1970; Friedman and Herndon, 1972). These and

similar experiments were interpreted using one of two different theories, the cyclotron maser instability (Sprangle and Manheimer, 1975) and stimulated Raman scattering (Sprangle et. al, 1975), which predicted large growth rates and high efficiencies. The cyclotron maser instability is a purely relativistic effect associated with relativistically gyrating electrons. This mechanism has been successfully used in the development of gyrotrons, relatively compact tube-type devices which operate at the fundamental or harmonics of the cyclotron frequency (See, e.g., Granatstein, ed., 1981). Stimulated scattering experiments, on the other hand, have continued to employ Marx generators at higher voltage and current levels in order to take advantage of the γ^2 frequency scaling and the growth rate scaling with current. After the Stanford group popularized the term "free electron laser" and the equivalence of the FEL and stimulated scattering mechanisms was shown (Kroll and McMullin, 1978; Sprangle et. al., 1979), the high current experiments also began to be referred to as FEL's.

The first high current, relativistic beam experiment to be interpreted as stimulated scattering was performed at the Naval Research Laboratory (Granatstein et al., 1974). In experiments designed to produce microwaves at $\lambda = 2$ cm via the cyclotron maser interaction, strong submillimeter radiation was also observed. A quantitatively consistent explanation was that some of the 2 cm radiation reflected off the output window and subsequently interacted with a sufficiently cold part of the 1.5 MeV beam to produce the high frequency scattered radiation. In a subsequent experiment designed to optimize this effect, 400 μm radiation was generated at a power of ~ 1 MW (Granatstein et al., 1977).

The next important step in the development of high current FEL's came in an experiment at Columbia University in which the high power electromagnetic pump was replaced by a periodic magnetic wiggler, or quasi-wave (Mross et al., 1976; Efthimion and Schlesinger, 1977). A 750 keV, 5 kA beam was used to generate ≥ 10 -100 kW of mm or cm radiation. Subsequent experiments at Columbia increased the millimeter wave power level to more than 1 MW (Marshall et al., 1977a). This group also performed mode structure, spectral, and growth rate measurements which indicated that the mechanism responsible for the observed output was weak pump Raman scattering (Marshall et al., 1977b; Gilgenbach et al., 1979).

These early experiments at NRL and Columbia led to a collaborative effort on NRL's VEBA generator in which a quasioptical cavity was used to provide feedback (McDermott et al., 1978). Approximately 1 MW of 400 μm radiation was coupled out of the cavity, and the output wavelength agreed with theoretical predictions for the $\gamma = 3.4$ beam. An important result of this experiment was the demonstration of line narrowing when feedback was introduced. The line width decreased from $\Delta\lambda/\lambda > 10\%$ to $\Delta\lambda/\lambda \approx 2\%$.

The efficiency ($< 0.03\%$) of these high current experiments was strongly limited by the poor beam quality. Also, researchers at MIT have shown that the output from such experiments can easily be dominated by cyclotron emission (Shefer and Bekefi, 1982). Consequently, the NRL VEBA group (Parker et al., 1982) designed an improved diode in which 90% of the diode current was removed from the beam with a collimator. The collimated 1.5 kA, 1.4 MeV beam had an instantaneous axial velocity spread of $\sim 0.1\%$. The beam was passed through a helical wiggler and generated ~ 35 MW of radiation at

$\lambda \approx 4$ mm. This power was $\sim 2.5\%$ of the propagated beam power. A strong frequency dependence of the output on the axial guide field was observed, with the highest output occurring at a field slightly above the cyclotron resonance.

Another recent collective regime experiment at Columbia University has been reported in which the electrons were given an initial transverse velocity before their injection into the wiggler (Grossman et. al., 1983). Output was observed at a frequency equal to the sum of the doppler shifted cyclotron and usual FEL frequencies; i.e., $\omega_0 \approx 2\gamma_z^2 (\Omega_0/\gamma + k_w v_z)$. In this experiment, < 1 MW of power at $\lambda \approx 1.5$ mm was generated. This mechanism was independently proposed by the MIT group, which called it a Lowbitron (McMullin and Bekefi, 1981), and experiments to study the effect are also underway there.

Finally, an important trend that is occurring in FEL research is an attempt to bridge the gap between the two current regimes. High current experiments are being scaled to higher voltages in an attempt to produce higher output frequencies and/or higher powers. In an experiment being undertaken on the ETA induction linac ($V \sim 4.5$ MV) at Livermore, a high current beam (~ 1 kA) is being used in an attempt to efficiently generate very high FEL output powers at $f \sim 100$ GHz (Prosnitz and Sessler, 1982). At the Naval Research Laboratory, a program is underway to develop compact high current, and high voltage accelerators, which could be used as FEL drivers (Roberson et al., 1982). The long pulse duration experiment reported here is part of that program and is scalable to high energies.

IV. FEL Operating Regimes

There are three regimes of free electron laser operation. The operating regimes can be characterized, in part, by the velocity distribution relative to the phase velocity of the pondermotive wave. A phase space plot is shown in Figure 1.

In the Raman regime the beam appears cold to the pondermotive wave. There are no particles in resonance with the wave. The amplitude of the wave is too small to trap any beam particles at $z=0$. As the wave grows in space, the amplitude becomes large enough to trap the beam particles, thus terminating the linear growth phase.

In the kinetic Compton regime, the beam appears warm to the pondermotive wave. There are particles in resonance with the pondermotive wave. The linear growth is proportional to the slope of the distribution function. This is a Landau type growth mechanism. Kinetic theory is required to describe the FEL process in this regime. The pondermotive wave is resonant with a range of particles, as indicated by the dashed lines in the figure. The growth mechanism of the FEL in this regime has a quantum mechanical analogy with Compton scattering. It is not a single particle effect, since it requires a kinetic description, and so it is referred to as kinetic Compton. The phase space plot shows the growth of the wave in space. Initially the wave amplitude is small compared to the width of the resonance. The pondermotive wave will grow until the amplitude becomes large enough to trap the resonant particles, thus terminating the linear growth phase.

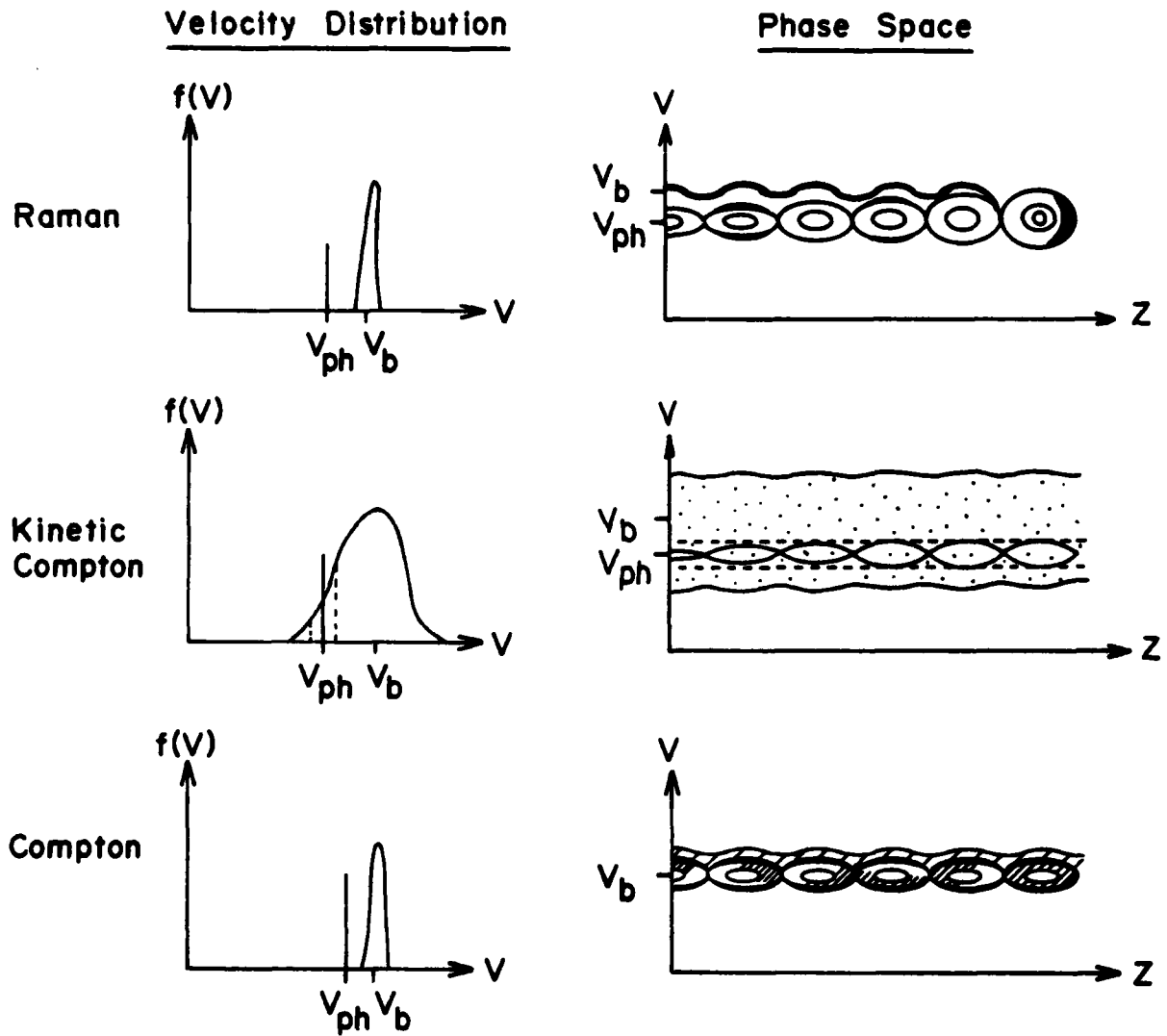


Figure 1. Velocity distributions and phase space plots of the three FEL operating regimes.

In the Compton regime, the beam energy is high and the current low. Single particle effects dominate over collective effects. The phase velocity of the pondermotive wave is less than the beam velocity. There are two modes in which a single particle Compton FEL may be operated. If the amplitude of the pondermotive wave is too small initially to trap the beam particles, as in the Stanford experiment, the gain is due to the perturbation of beam particles by the pondermotive wave. The interchange between wave and particle energy is oscillatory at the same period as the pondermotive wave. These particles are represented by a shaded region above the pondermotive wave ellipses in Fig. 1.

If the wave amplitude is sufficiently large, as in the Los Alamos experiment (Warren et. al., 1982), some or all of the beam particles may be trapped in the potential well of the pondermotive wave. The gain of the FEL in this region is due to the loss of particle energy as the particles rotate in the potential troughs of the pondermotive wave. This occurs at the trapped particle bounce frequency. The maximum gain is obtained when the beam particles are at the bottom of the ellipse in phase space.

The efficiency of the free electron laser can be increased in all of these schemes by decreasing the phase velocity of the pondermotive wave after it has trapped the beam particles. The decrease in particle energy appears as an increase in wave energy.

To operate a high current beam in the Raman regime requires

$$\frac{\Delta\gamma}{\gamma} < \frac{\omega_b}{\gamma^{3/2} c k_w} \quad (10)$$

where ω_b is the beam plasma frequency (Sprangle et al., 1979). Combining this with $\lambda = \lambda_w/2\gamma^2$ gives

$$\lambda > \frac{c\pi}{\omega_b \gamma^{1/2}} \cdot \frac{\Delta\gamma}{\gamma} \quad (11)$$

This condition can be shown to be equivalent to requiring $\lambda' > \lambda'_D$, where λ' and λ'_D are the wavelength and Debye length in the beam frame (Hasegawa, 1978). The energy spread $\Delta\gamma/\gamma$ which results from the normalized emittance ϵ_n of a beam with radius r_b is (Neil, 1977)

$$\frac{\Delta\gamma}{\gamma} = \frac{1}{2} \frac{\epsilon_n^2}{r_b^2} \quad (12)$$

The Lawson-Penner relation which relates the emittance to the beam current is

$$\epsilon_n^2 = S^2 I(\text{kA}) \text{ (cm - rad)} \quad (13)$$

where S is a scale factor that is typically 0.1 - 0.3 for existing accelerators.

Combining these equations we find for a Raman interaction, that

$$\lambda(\text{cm}) > 5.7 \frac{S^2}{\gamma^{1/2}} J^{1/2} \text{ (kA/cm}^2\text{)} \quad (14)$$

At a current density of 1 kA/cm² and $S = 0.3$ the wavelength must be greater than 0.3 cm to operate in the Raman regime when $\gamma = 3$. To operate a 1 micron FEL in the Raman regime for such a beam would require $\gamma = 2600$, or

1.3 GeV, and a wiggler with a wavelength of 135 meters. Consequently, the Raman FEL is not viable in the IR region unless S can be greatly reduced.

It is clear from Eq. 14 that there are three parameters one can improve upon to extend the Raman region. The kinetic energy of the beam can be increased, the current density decreased or the scale factor in the emittance relation decreased. However, there is a limit to the extent one can increase the energy, decrease the current density and maintain a collective interaction. When the number of particle in the debye sphere is small, the system will not support collective oscillations.

The wavelength condition of Eq. 14 is most sensitive to S , so it is important to analyze the degree to which S can be reduced. The Lawson-Penner relation is not derived from first principles but is a phenomenological relation which has been shown to hold in many accelerators. The success of the Lawson-Penner relation is related to the fact that the reliable current density from oxide thermionic cathodes is generally $< 10 \text{ A/cm}^2$. With higher current density cathodes, the scale factor, S , can be reduced considerably. In a recent experiment using cold graphite cathodes, an S parameter of 0.12 was obtained with a 14 kA beam by aperturing the beam to about 30 percent of the diode current (Sloan et al, 1982). An S parameter of .13 at 4 kA was obtained by aperturing to about 25% of the current from a spiral knife-edge cold cathode in a 20 MeV induction linac (Kulke et al., 1981). Finally, a much reduced value of $S = 0.04$ at 1.5 kA was calculated for a recent experiment in which only $\sim 5-10\%$ of the current from a graphite cold cathode was extracted from the diode (Parker et al., 1982).

The S parameter is best understood in terms of the brightness, another invariant that is related to the emittance:

$$B_n = \frac{I}{\pi^2 \epsilon_n^2} = \frac{1}{\pi^2 S^2} = \frac{J}{2\pi \Delta\gamma/\gamma} . \quad (15)$$

Thus, the brightness is a measure of our ability to make a high current density, cold beam. To the extent that the emittance is an invariant, the brightness is determined at the diode; hence if we compress the beam at a later stage we increase $\Delta\gamma/\gamma$. Therefore, for high power operation it is desirable to have a high current density cathode. From the above three experiments we can conclude that the brightness of cold cathodes with appropriate aperturing is a factor of six to sixty higher than that of hot cathodes. This will extend the Raman wavelength region by a corresponding amount. However, the price one pays for cold cathode operation is diode closure. This can limit the pulse length to a few hundred nanoseconds. In addition, the efficiency of the system is reduced by a factor of 5 to 10 when a large fraction of the beam is terminated by aperturing.

The emittance is often the dominant contributor to energy spread. However, the self potential and the wiggler gradient can also contribute to the beam energy spread, which in general is given by

$$\frac{\Delta\gamma}{\gamma} = \frac{1}{2} \frac{\epsilon_n^2}{r_b} + \frac{1}{\gamma_0} \left(\frac{r_b \omega_b}{2c} \right)^2 + \left(\frac{r_b \Omega_w}{2c} \right)^2 , \quad (16)$$

where the second term is the contribution from the self potential and the third is from the wiggler gradient. From this we can find an optimum radius of

$$r_b^4 = \frac{2c^2 \epsilon_n^2}{\omega_b^2 / \gamma_0 + \Omega_w} . \quad (17)$$

For high current beams propagated in a strong axial magnetic field, the equilibrium radius (Neil, 1977) should be compatible with the optimum radius.

The variation in γ as determined by the emittance, wiggler gradients and self field of the beam results in a velocity spread of the beam that is independent of time. If the diode voltage is time dependent (as for example due to diode closure), this will shift the output wavelength. If the gain is sufficiently high in an oscillator the time variation will cause a broad band output. The time variation in an amplifier experiment can cause a loss of resonance with the input signal. The range of unstable wave numbers is (Sprangle et. al., 1979)

$$\Delta k = 8 k_i^2 / k , \quad (18)$$

where k_i is the spatial growth rate. This can be related to the variation in γ through $\lambda = \lambda_w / 2\gamma^2$. Then $\frac{\Delta\gamma}{\gamma}|_t < 4 k_i^2 / k^2$ is required. Substituting

the maximum growth rate value for k_i^2 we get

$$\left. \frac{\Delta\gamma}{\gamma} \right|_t < 2\gamma^{1/2} \frac{\Omega_w^2 u_b^2}{(2\pi c)^3} \lambda^3 \quad (19)$$

Therefore, the requirements on the time variation of the beam energy to keep the growth of the output wavelength in the unstable region is proportional to λ^3 . For a 1 kA/cm², 1 MeV beam in a 1 kG wiggler field an output wavelength of 0.7 mm requires a $\Delta\gamma/\gamma$ time variation of less than 1%.

V. Accelerator Development

During the past fifty years accelerators have developed primarily along two directions: (1) low current, high voltage and (2) high current, low voltage devices. Consequently FEL research has followed similar lines. The history of traditional accelerators is quite well known. The average current in these accelerators is generally less than an ampere with micro bunch currents reaching tens of amperes. The energies achieved in electron linacs exceeds 10^{10} eV and the beam energy in a proton synchrotron is approaching 10^{12} eV. High current accelerators have been developed primarily as Marx generators driving a pulse forming line, which is connected to a diode. The energy of these devices is typically around 1 MeV, although 10 MeV devices have been built. The pulse current from a pulse-power line diode has reached 10 MA. These devices do not scale well in energy because the total energy is achieved in a single gap, hence the stress on the insulator becomes excessive at high voltages. A free electron laser requires high voltage for

short wavelength operation and high current for efficiency and high gain. Only the induction linac has been a serious candidate as a FEL driver in this parameter range. Experiments at Lawrence Livermore Laboratory on the Experimental Test Accelerator (ETA) have achieved currents approaching 10 kA and beam energies of 5 MeV. A scaled up version of this accelerator is designed for 50 MeV, 10 kA, 30 ns operation. The current from this device is probably excessive for efficient FEL operation and the pulse length too short.

A long pulse induction linac ($\tau = 2 \mu\text{sec}$) was built at the National Bureau of Standards (Leiss, et al., 1980) and is currently in operation at the Naval Research Laboratory. Figure 2 is a schematic of the Long Pulse Induction Linac. The accelerator consists of two major components; (1) an injector and (2) an induction accelerator module.

The electron gun in the injector has a 16.5 cm diameter tungsten dispenser thermionic cathode. Electrons are accelerated in the gun through a series of 12 annular electrodes, spaced by ceramic insulator rings. The last electrode supports a 95% transmission tungsten mesh at ground potential. The gun has also been operated with a graphite brush cold cathode (Ramirez and Cook, 1980; Prohaska and Fisher, 1982).

The electron gun is immersed in an oil filled tank. The gun voltage is fed from a pulse line driving a 12:1 step up transformer. The injector typically produces a 0.8 kA beam pulse of 400 keV. The electron beam is transported to the induction accelerator module by a series of focusing coils.

INDUCTION LINAC

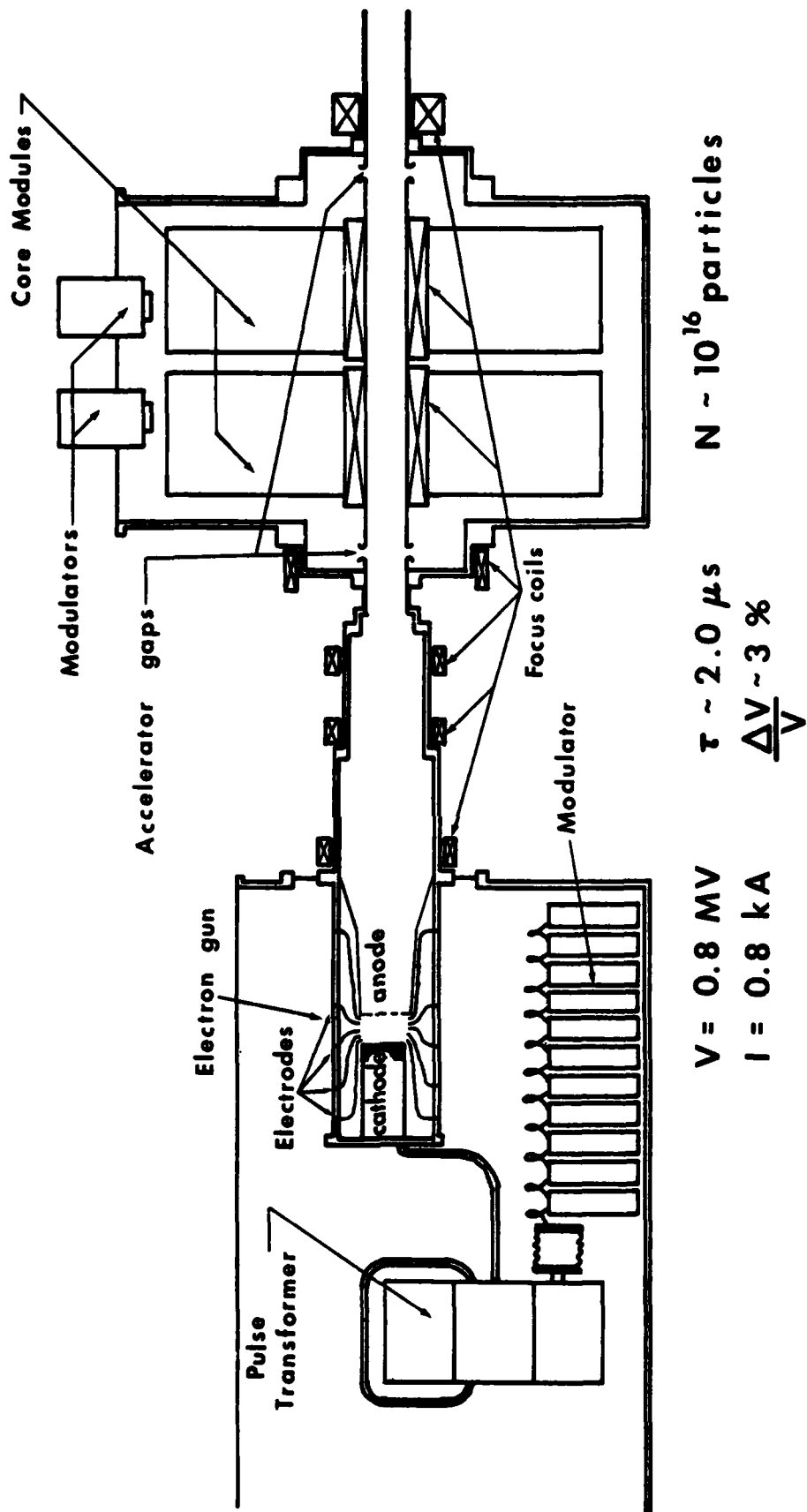


Figure 2. Schematic of Long Pulse Induction Linear Accelerator.

The induction accelerator module consists of two core sets. One of the core sets give a 4 to 1 step up voltage and the other a 5 to 1. The cores are wound with 0.001 inch mild steel foil, separated by 0.00025 inch mylar sheets. Each accelerating gap produces about 200 kV of acceleration.

Typically, the output energy of the electron beam generated by the linac is 0.8 MeV, the current approximately 0.8 kA and the pulse length 2 μ sec. However, for the data reported in this work one of the accelerating gaps was not operating, so the beam voltage was 0.55 MeV. Also, a graphite brush cold cathode was used and the 0.8 kA diode current was reduced to 0.2 kA due to losses in beam transport. The temporal variation in the voltage with the hot cathode is less than 3 percent over 1.6 μ sec. This is the longest pulse induction linac in existence, with a pulse duration more than an order of magnitude longer than other induction linacs. The pulse length becomes an important consideration for free electron laser experiments where one wishes to study the nonlinear dynamics of the beam or efficiency enhancement schemes. Applications that require a significant amount of energy in the radiation field also require long pulses to avoid the problems encountered with excessive electric field strengths at short pulses.

Figure 3a shows the voltage and current traces of the injector for the long pulse induction linac. The voltage remains constant to within a few percent over the 2 microsecond pulse length. In contrast Figure 3b shows the voltage and current from the graphite cathode diode of the Febetron, a relatively long pulse Marx type generator. The oscillations on the voltage and current are due to the finite element pulse line of the Febetron Marx. The diode voltage decreases 25 percent in 250 nsec as a result of diode

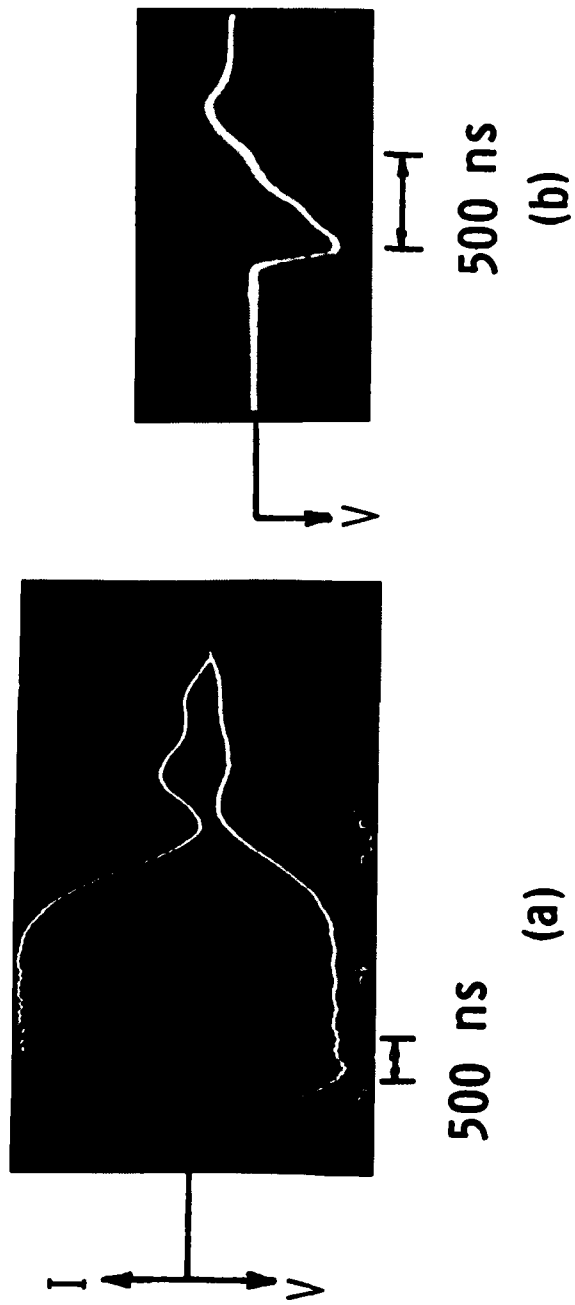


Figure 3. Comparison of diode waveforms with hot (a) and cold (b) cathodes.

closure. This closure-induced voltage collapse is typical of cold, plasma cathodes, and in light of the condition of Eq. 19, is a key problem for long pulse FEL operation. Efforts to prevent diode closure, such as magnetic insulation, generally result in higher beam emittance.

The relationship between the cathode plasma velocity and the diode parameters can be determined by considering the simple circuit shown in Fig. 4. There is a voltage source V_C , an internal line impedance Z_L , and a time dependent diode impedance $Z_D(t)$. The current is

$$I = V_C / (Z_L + Z_D). \quad (20)$$

The diode voltage is

$$V_D = IZ_D = V_C Z_D / (Z_L + Z_D) \quad (21)$$

and the diode impedance is

$$Z_D = \frac{ad^2(t)}{v_D^{1/2}}, \quad (22)$$

where a is a constant and d the anode cathode spacing. We will assume

$$d = d_0 - \alpha t \quad (23)$$

where α is the plasma closure velocity. The closure velocity for high current cold cathodes is typically ~ 2.5 cm/ μ s. Now if we differentiate Eq. (21)

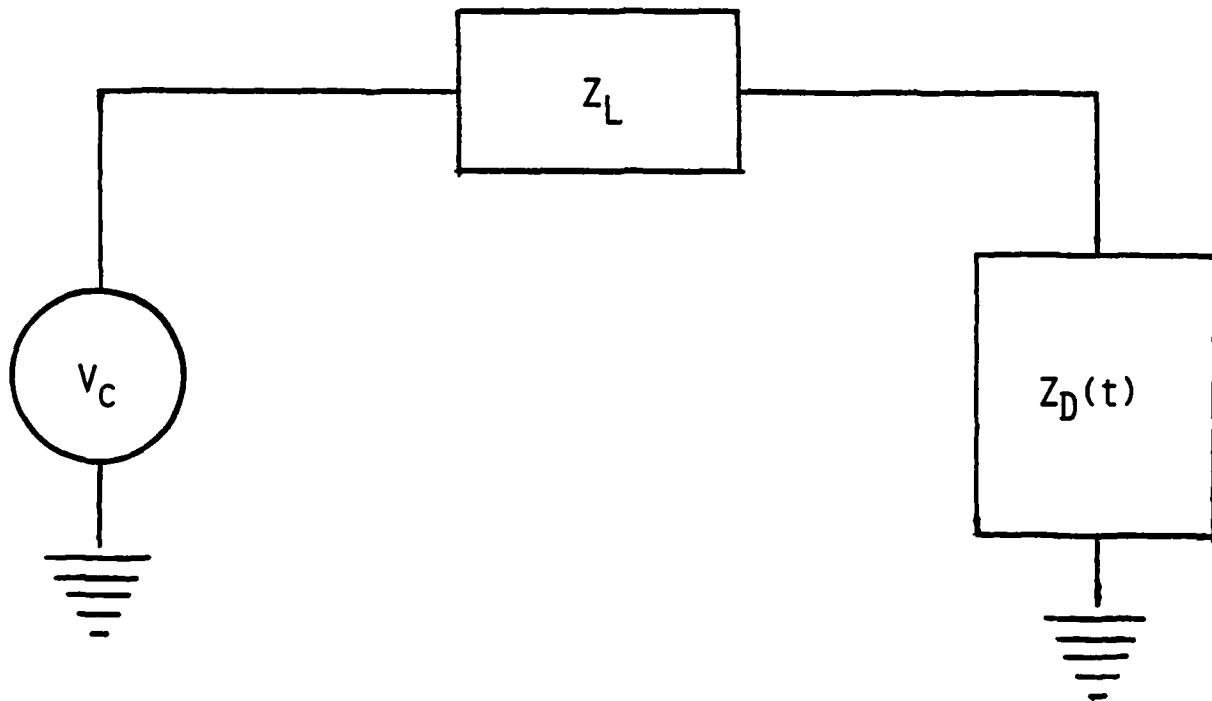


Figure 4. Idealized circuit diagram of an electron beam generator. Source voltage V_c appears across line impedance Z_L in series with diode impedance Z_D .

with respect to time and assume the diode impedance is matched to the line at $t = 0$, then $V_C = 2 V_D$ and

$$\frac{\Delta V_D}{V_D} = \frac{1}{2} \frac{\Delta Z_D}{Z_D} \quad (24)$$

$$\Delta Z_D = \frac{2ad\Delta d}{V_D^{1/2}} - \frac{1}{2} \frac{ad^2 \Delta V_D}{V_D^{3/2}} \quad (25)$$

Then

$$\frac{\Delta V_D}{V_D} = \frac{4}{5} \frac{\Delta d}{d} \quad (26)$$

and

$$V_D(t) = V_D(0) \left(\frac{d}{d_0}\right)^{4/5} = V_D(0) \left(1 - at/d_0\right)^{4/5} \quad (27)$$

Hence for a diode that is initially matched we can obtain a simple expression for the time dependence as a function of diode spacing.

Figure 5 is a plot of the diode voltage as a function of time for $Z_L = Z_D$, $Z_L = 10 Z_D$ and $Z_L = 0.1 Z_D$ when $t = 0$. When the line impedance is ten times the diode impedance, the device tries to behave as a constant current source and the voltage decays faster than in the matched load case. When the line impedance is small compared to the diode impedance, the device tries to act as a constant voltage source at the expense of an increased current. However,

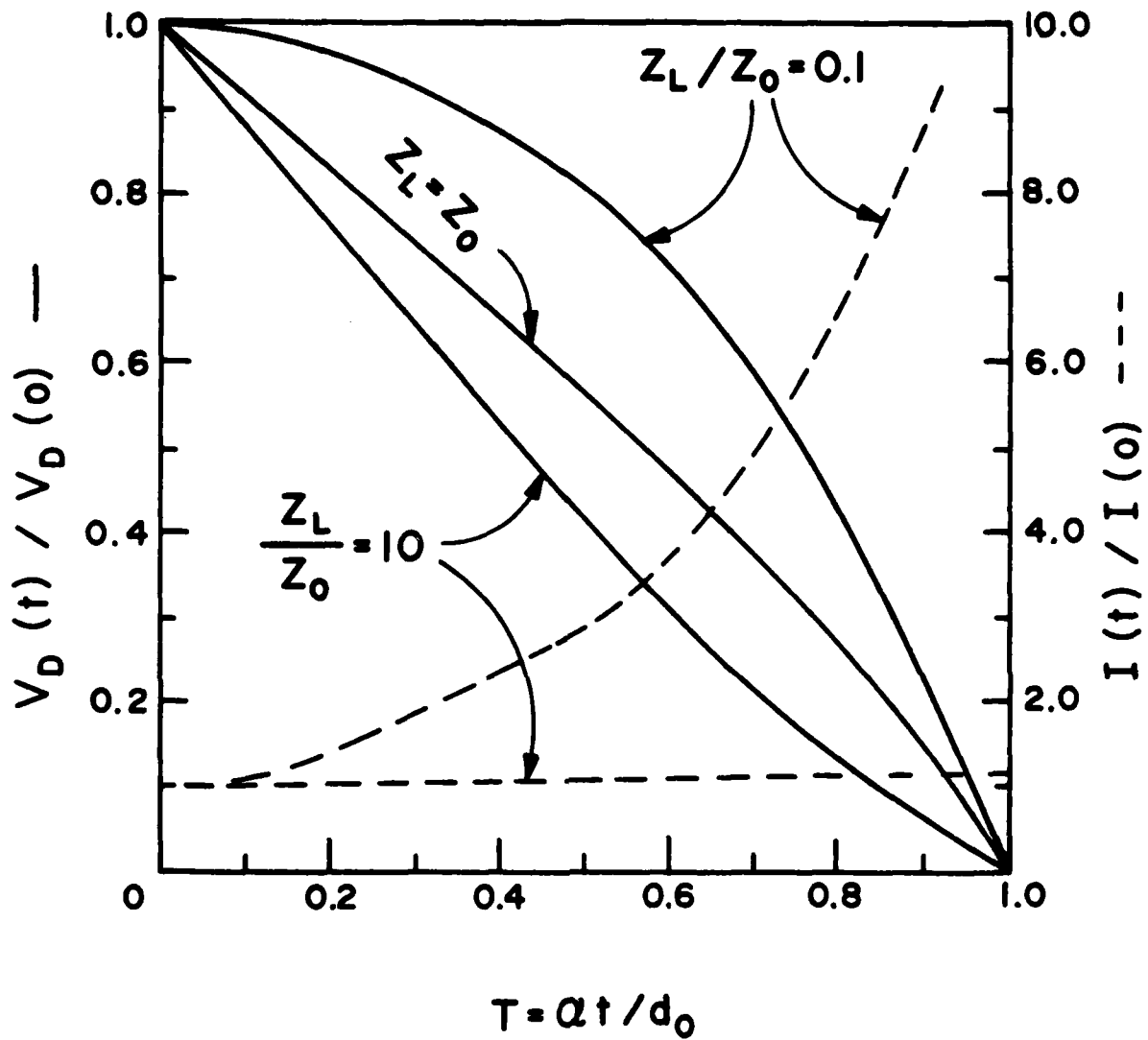


Figure 5. Calculated diode voltage and current for three different diode impedances. The line impedance is Z_L and Z_0 is the diode impedance at $t = 0$.

for high current beams, the increasing self potential of the beam with current will cause the beam's kinetic energy to decrease faster than the diode voltage.

Although diode closure in high current cold, cathode machines is a limiting factor for long pulse operation, there are many operational advantages to cold cathodes. Thus, we have temporarily replaced the hot cathode in the induction linac with a graphite brush cold cathode of the same area. The average electric field at the cathode surface is about 30 kV/cm. The cathode rapidly turns on, and the closure problem does not seem to be as severe as in the Febetron. Perhaps the large area, low current density reduces the closure velocity. The emittance is worse than with the hot cathode, and more of the beam is lost in transport. However, the emittance of the beam transported to the wiggler appears to be about the same as with the hot cathode.

VI. The FEL Apparatus

Figure 6 is a sketch of the free electron laser experiment. There is a uniform axial field of 120 cm length which is varied from 1 to 5 kG, with a typical operating field of 2 kG. The beam from the induction linac is focused into the solenoid. The experiment has not yet been run with the mirrors in place as shown, but operated in a superradiant mode.

Two wiggler configurations have been investigated: (1) a pulsed linear wiggler and (2) a radially symmetric diffusive wiggler. The amplitude of the linear wiggler field can be varied from 0.1 kG to 1 kG. The wiggler

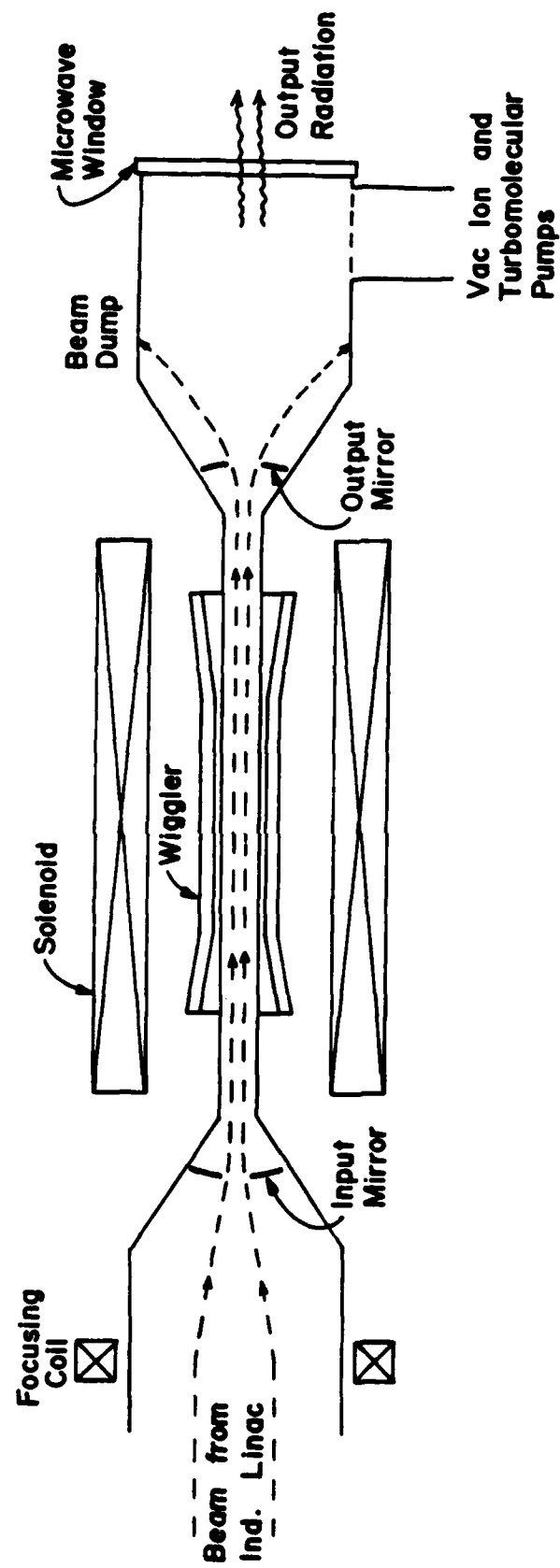


Figure 6. Schematic of FEL interaction region.

wavelength in 3.0 cm, and the overall length of the wiggler is 120 cm. The wiggler amplitude rises adiabatically in 30 cm, has a uniform straight section of 60 cm and decays adiabatically in the last 30 cm.

Two diffusive wigglers have been used: a 6 cm period aluminum wiggler and a 4.5 cm copper wiggler. The perturbed axial component of the on-axis field is 4 percent of the axial field for the 6 cm wiggler and 6 percent for the 4.5 cm wiggler.

The output radiation is extracted through a large area window, and the power and spectrum are determined by gas breakdown thresholds or with high pass filters and calibrated detectors.

A. Linear Wigglers

There are several advantages to linear wigglers, including ease of assembly, changing the periodicity to operate at different wavelengths, and tapering the period and/or field amplitude for efficiency enhancement (Sprangle et al., 1979). As a result of our experiments and analysis, we find that a linear wiggler in an axial guide field produces an elliptical polarization. The ratio of the major to minor axis of the ellipse is $k_w v_z / \Omega_0$, where k_w is the wiggler wave number, v_z the axial beam velocity, and Ω_0 the cyclotron frequency in the axial guide field. As a result of the asymmetry of the wiggler, there are no focusing forces in one of the directions perpendicular to the beam propagation and an electron drift results. Although this drift can be very small in some parameter regimes, it is always present in linear wigglers immersed in an axial guide field unless additional focusing

forces are provided. This problem was avoided in a high current device using a linear wiggler by eliminating the solenoidal field (Phillips, 1960). Focusing was provided by increasing the wiggler field at the edges.

To understand how the elliptical polarization and perpendicular drift arise, we will solve the equations of motion in the combined wiggler and axial fields. The linear wiggler field components are

$$\begin{aligned}
 B_{wx} &= 0 \\
 B_{wy} &= b(z) B_w \cosh k_w y \cos k_w z \\
 B_{wz} &= -b(z) B_w \sinh k_w y \sin k_w z
 \end{aligned}
 \tag{28}$$

where B_w is the peak wiggler field on axis and $b(z)$ is an adiabatic taper in the wiggler amplitude at the entrance and exit of the wiggler. The amplitude increases to its full value in ten periods in our experiment.

We define $\Omega_0 = qB_0/\gamma m$ and $\Omega_w = qB_w/\gamma m$. To simplify the analysis we will make the following assumptions

$$\frac{B_w}{B_0}, \frac{v_x}{v_z}, \frac{v_y}{v_z}, k_w y \ll 1
 \tag{29}$$

and $v_z \approx v_b \approx \text{constant}$. The single particle equation of motion then gives

$$\dot{v}_x = (\Omega_0 v_y - \Omega_w \cosh k_w y \cos k_w z v_z)$$

$$\dot{v}_y = -v_x \Omega_0 \quad (30)$$

$$\dot{v}_z = v_x \Omega_w \cosh k_w y \cos k_w z$$

where we have neglected the correction to B_z from the wiggler since $B_w/B_0 \ll 1$ and $v_y \ll v_z$.

We take the derivative of each of the components with respect to time and use the assumptions of Eq. 29 to get

$$\ddot{v}_x + \Omega_0^2 v_x = \Omega_w k_w \cosh k_w y \sin k_w z v_z^2. \quad (31)$$

Similarly

$$\ddot{v}_y + \Omega_0^2 v_y = \Omega_0 \Omega_w \cosh k_w y \cos k_w z v_z \quad (32)$$

We have the following solutions

$$v_x = \frac{\Omega_w k_w \cosh k_w y \sin k_w z v_z^2}{\Omega_0^2 - k_w^2 v_z^2}$$

$$v_y = \frac{\Omega_0 \Omega_w \cosh k_w y \cos k_w z v_z}{\Omega_0^2 - k_w^2 v_z^2}$$

$$v_z = \frac{\Omega_w v_x \cosh k_w y \cos k_w z}{\Omega_0^2 - k_w^2 v_z^2}$$

(33)

$$y = \frac{\Omega_0 \Omega_w \cosh k_w y \sin k_w z}{k_w (\Omega_0^2 - k_w^2 v_z^2)}$$

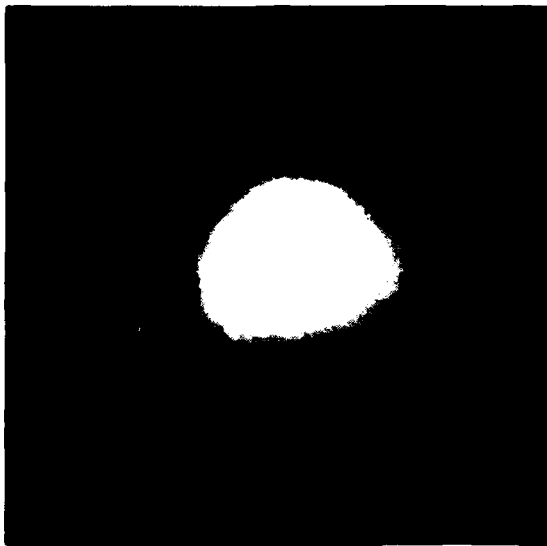
The displacement in the x direction is proportional to the wiggler field and axial velocity. The displacement in the y direction occurs only if there is a nonzero solenoidal magnetic field. It is proportional to both the solenoidal and wiggler field. This displacement is a result of the Lorentz force arising from the x-component of v_w and B_0 .

The ratio of the maximum excursion in the x-direction to that in the y-direction is seen from Eq. 33 to be

$$\Delta x / \Delta y = k_w v_z / \Omega_0. \quad (34)$$

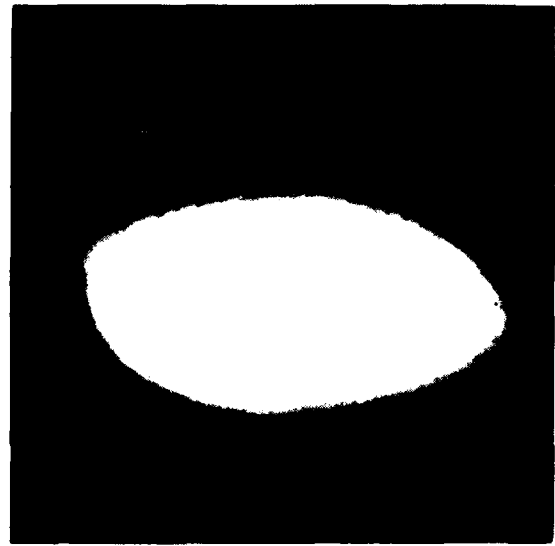
Thus, this ratio is a measure of how close Ω_0 is to the cyclotron resonance which occurs at $\Omega_0 = k_w v_z$. Since $k_w v_z$ is approximately constant in the experiment, the ratio of the maximum displacements $\Delta x / \Delta y$ should vary as $1 / \Omega_0$.

Figure 7 is a series of exposures made from x-rays produced when the beam strikes a target placed beyond the wiggler. These photos give us the shape of the beam versus solenoidal field. In Fig. 7(a), the wiggler field is zero and the beam is approximately circular. In Fig. 7(b), with a 500 Gauss wiggler field the beam becomes elongated in the x-direction. The linear wiggler field is in the y direction, consistent with the above analysis. As the solenoidal field is increased with the wiggler field constant, the shape goes from



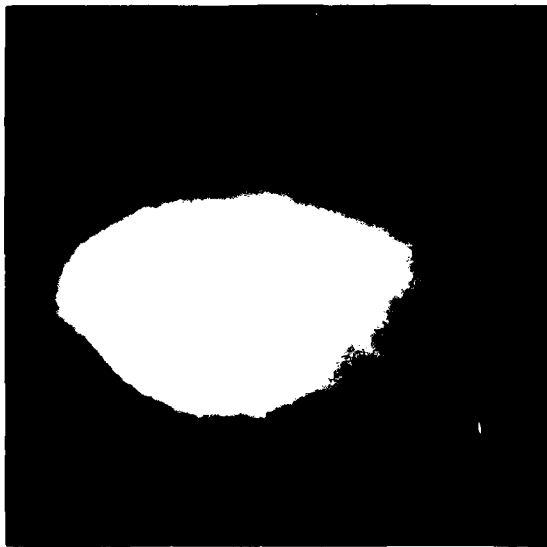
$B_0 = 1.74 \quad B_W = 0$

(a)



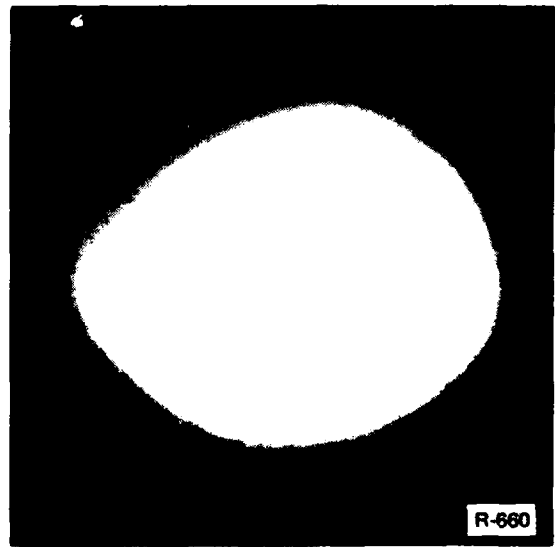
$B_0 = 1.74 \quad B_W = 0.5$

(b)



$B_0 = 2.6 \quad B_W = 0.5$

(c)



$B_0 = 3.48 \quad B_W = 0.5$

(d)

Figure 7. Time integrated x-ray exposure of beam striking a target placed beyond linear wiggler (wiggler field is vertical) for various values of solenoidal field.

elliptical to circular, as shown in Figs. 7(b) - 7(d). Hence, we would expect a nearly linearly polarized output for (b) and a nearly circular polarization for (d).

Figure 8 is a plot of the ratio $\Delta x/\Delta y$ as a function of the solenoidal field. The results are plotted three ways. The solid line is the theory, the small dots were computed numerically and the circled x points are experimental. At small values of magnetic field the approximations break down and there is a large variation in the results.

We have demonstrated that the polarization of a linear wiggler in a solenoidal magnetic field may be varied by changing the magnitude of the solenoidal field. In addition, we see from Eqs. 34 that a change in the amplitude of the wiggler field alone does not change the polarization. We have confirmed this by propagating a beam the entire length of the wiggler in a solenoidal magnetic field of 2 kG. The wiggler field is varied up to 1 kG without changing the shape or intensity of the beam.

As a result of the asymmetry of the wiggler, there are no focusing forces in the x-direction. This results in a net drift of off axis particles (Pasour et al., 1982). This drift is shown clearly in Fig. 9, which consists of electron trajectories in the x-y plane. The trajectories are calculated by numerically solving the equations of motion, including self-fields. Initially the electrons $\vec{E} \times \vec{B}$ drift azimuthally as they are injected into to the adiabatically increasing wiggler field. However, when they reach the constant amplitude portion of the wiggler, the electrons drift rapidly in a direction perpendicular to both the axial and wiggler fields.

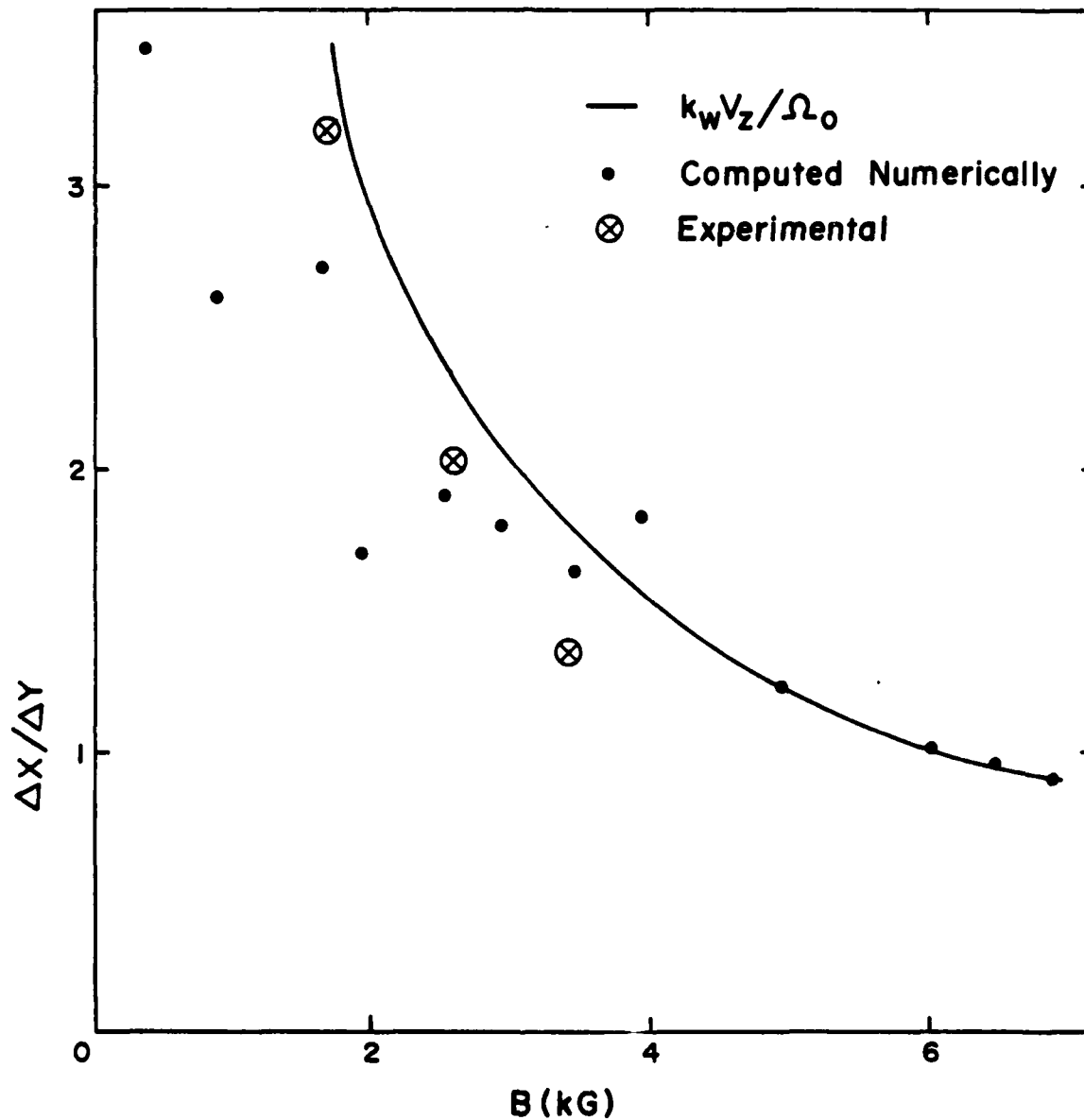


Figure 8. Plot of beam elongation ($\Delta x/\Delta y$) vs. axial magnetic field in a linear wiggler (B_w in y-direction). Solid line is theoretical curve (Eq. 34), dots are values obtained by numerical integration of orbit equations, and crosses are experimental results.

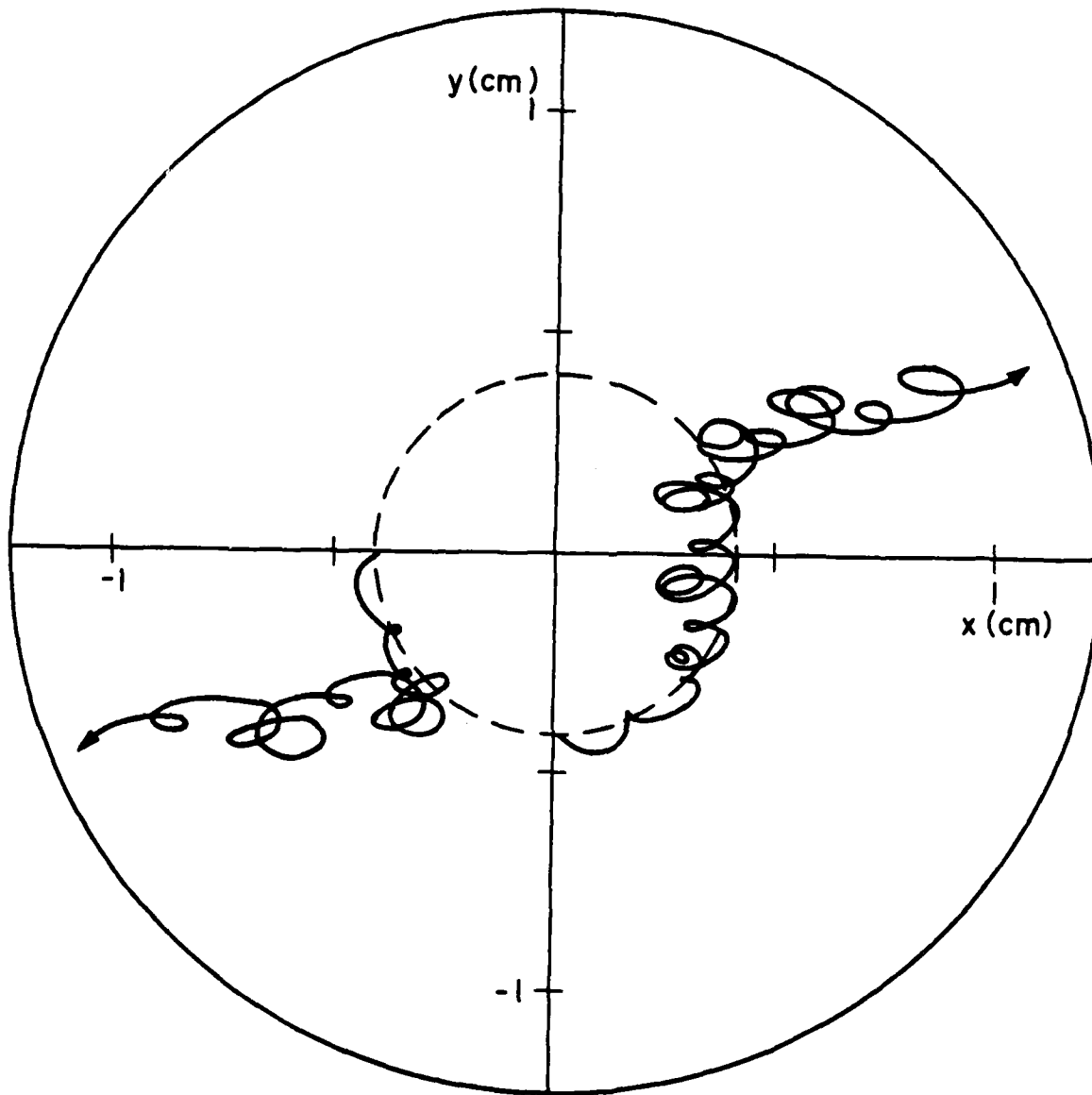


Figure 9. Electron trajectories in a linear wiggler and an axial magnetic field. In this case, $B_w = 1$ kG, $B_o = 250$ A, $\lambda_w = 3$ cm, and $\gamma = 2.2$.

An approximate, empirical expression for the drift has been found which is in good agreement with results from computer calculations of the electron orbits when $\Omega_w < \Omega_o < kv_z$. In terms of the wiggler gradient, the expression is

$$\vec{v}_d = \frac{1}{2} \frac{v_{\perp}^2}{\Omega_o} \cdot \frac{\nabla(\vec{B}_w)^2}{2(\vec{B}_w)^2} \times \frac{\vec{B}_o}{B_o}, \quad (35)$$

where $v_{\perp}^2 = v_x^2 + v_y^2$. This expression has the same form as the usual grad B drift and can be thought of as arising from the crossed wiggler gradient and axial field. It can also be written as

$$v_d = \frac{1}{2} v_z \frac{k_w v_z}{\Omega_o} \cdot \frac{(\Omega_w k_w v_z)^2 \cosh k_w y \sinh k_w y}{(\Omega_o^2 - k_w^2 v_z^2)^2} \quad (36)$$

This expression is reasonably valid for $k_w y \leq 0.8$, $B_{wy} \gg B_{wz}$, and

$v_{\perp} \ll v_z$. Note that the drift is very small near the axis but increases exponentially with $k_w y$.

Table 1 compares drift velocities for various cases as calculated by the computer trajectory code to those calculated from the Eq. 36. In general the agreement is very good. One consequence of the large drift near resonance is that it limits the degree of gain enhancement achievable through the magneto-resonance effect.

TABLE I

Comparison of drift velocities computed from the code with those from Eq. 9 for various cases.

B_o (kG)	B_w (kG)	γ	$\frac{\Omega_o}{kv_z}$	X(cm)	$\frac{v_d}{c}$ (code)	$\frac{v_d}{c}$ (Eq. 9)
2	1	2.2	0.29	0.4	0.047	0.050
4	1	2.2	0.57	0.4	0.042	0.046
2	0.5	2.2	0.29	0.4	0.011	0.013
2	1	2.2	0.29	0.2	0.019	0.022
2	1	3.0	0.21	0.4	0.029	0.034
4	1	3.0	0.42	0.4	0.019	0.022
4	0.5	3.0	0.42	0.4	0.0051	0.0056
4	1	10.0	0.11	0.4	0.0043	0.0049
10	5	10.0	0.28	0.4	0.057	0.056

B. Helical Wiggler

Because the linear wiggler drift is so sensitive to slight off-centering or large diameter of the beam, a helical wiggler would seem to be somewhat better suited to the experiment, at least initially when beam focusing is not optimized. If the trajectory calculation is repeated with the same parameters as those in Fig. 9 but with a helical wiggler substituted for the linear one, it is found that the electron drifts azimuthally and is well confined, as shown in Fig. 10 (Pasour et al., 1982). This behavior results from the radially increasing wiggler field, which for $k_w r \lesssim 0.8$ can be written as (Blewett and Chasman, 1977)

$$B_r = B_w \left(1 + \frac{3}{8} k_w^2 r^2\right) \sin(\theta - k_w z)$$

$$B_\theta = B_w \left(1 + \frac{1}{8} k_w^2 r^2\right) \cos(\theta - k_w z) \quad (37).$$

$$B_z = -kr B_w \left(L + \frac{1}{8} k_w^2 r^2\right) \cos(\theta - k_w z).$$

Although a helical wiggler is in general more difficult to construct than a linear one and is not nearly as amenable to tapering, the orbital stability that it provides is a major advantage when an axial guide field is used. Also, it is possible to taper the amplitude of the wiggler field in the helical wiggler by carefully varying the winding radius as a function of z .

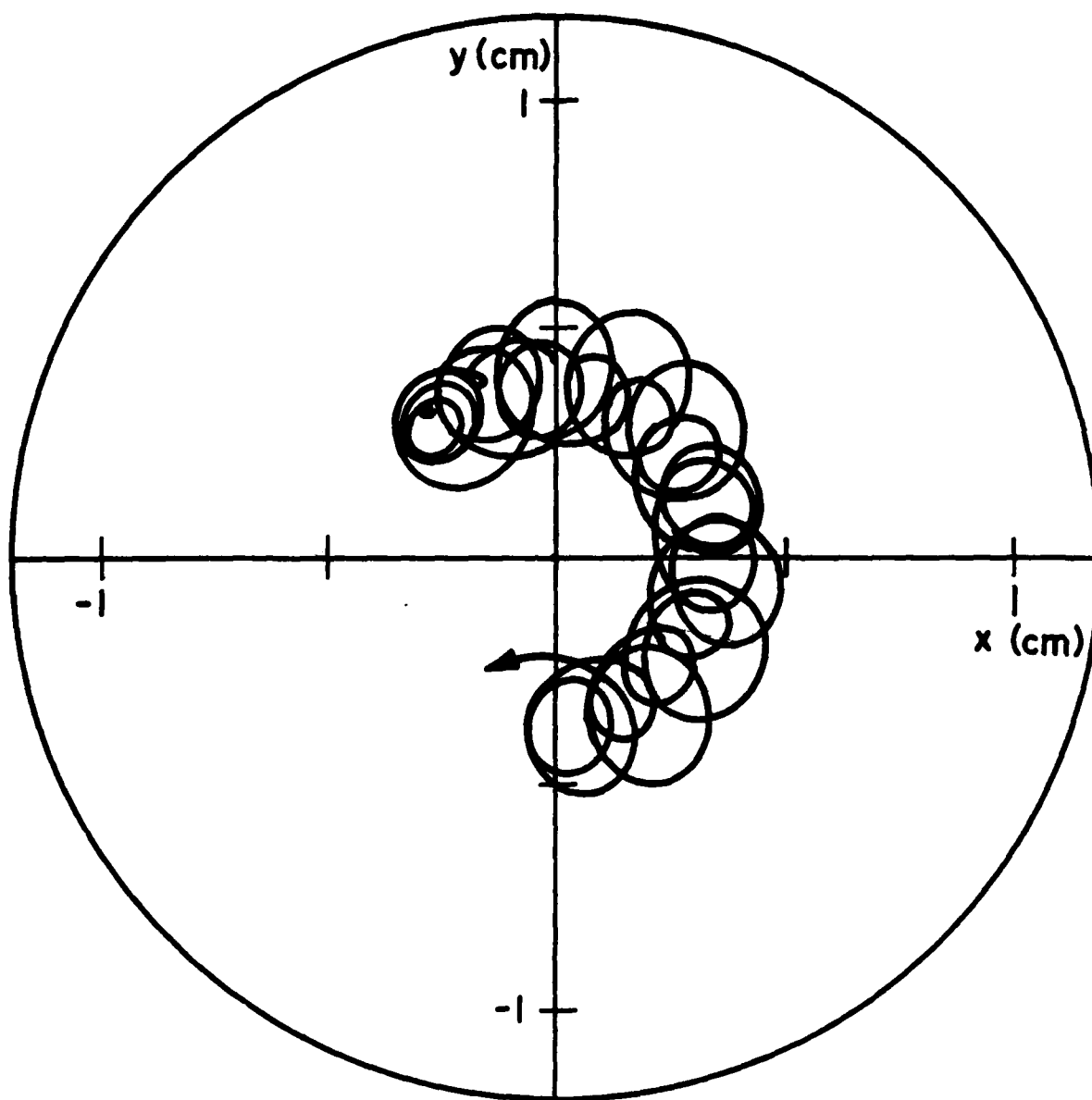


Figure 10. Electron trajectories in a helical wiggler and an axial magnetic field. Parameters are identical to those in Figure 9.

C. Diffusive Wiggler

An axially symmetric wiggler can be constructed by placing conducting rings in a pulsed solenoidal magnetic field (Jacobs et al., 1980). As the solenoidal field diffuses in, it induces eddy currents in the conducting rings which generate an opposing field. This results in a magnetic field with a periodic radial component. This process is illustrated in the computer plots of Fig. 11.

The magnetic field at a distance r from the the axis is approximately

$$\vec{B} = \hat{z} [B_0 + B_1 I_0(k_w r) \sin(k_w z)] - \hat{r} B_1 I_1(k_w r) \cos(k_w z) , \quad (38)$$

where I_0 and I_1 are modified Bessel functions and B_1 is the amplitude of the axial field modulation on axis.

Figure 12 is a computer plot of the axial component of the magnetic field of the diffusive wiggler used in the system. When the wiggler is not present, the solenoidal field is 2 kG. Hence, the wiggler not only modulates the solenoidal field, it reduces the average value. To make a smooth transition into the wiggler field, the conducting rings extend all the way to the end of the solenoid where the field drops to one half the peak value.

Since the diffusive wiggler is axially symmetric, it does not produce the kind of radial particle drift which is characteristic of linear wigglers in an

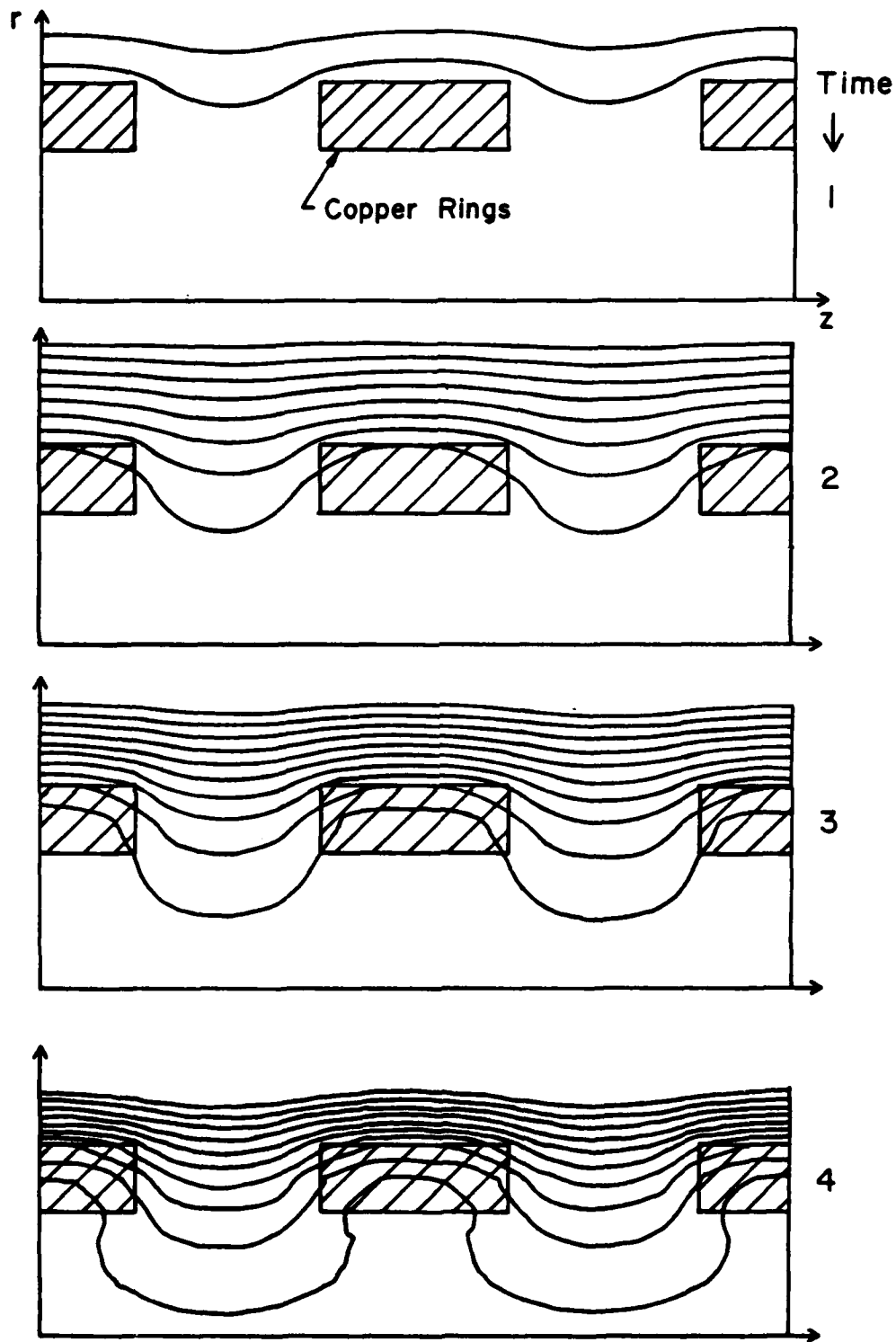


Figure 11. Diffusion of magnetic field through copper rings used in diffusive wiggler. Plots show field lines at progressively later times.

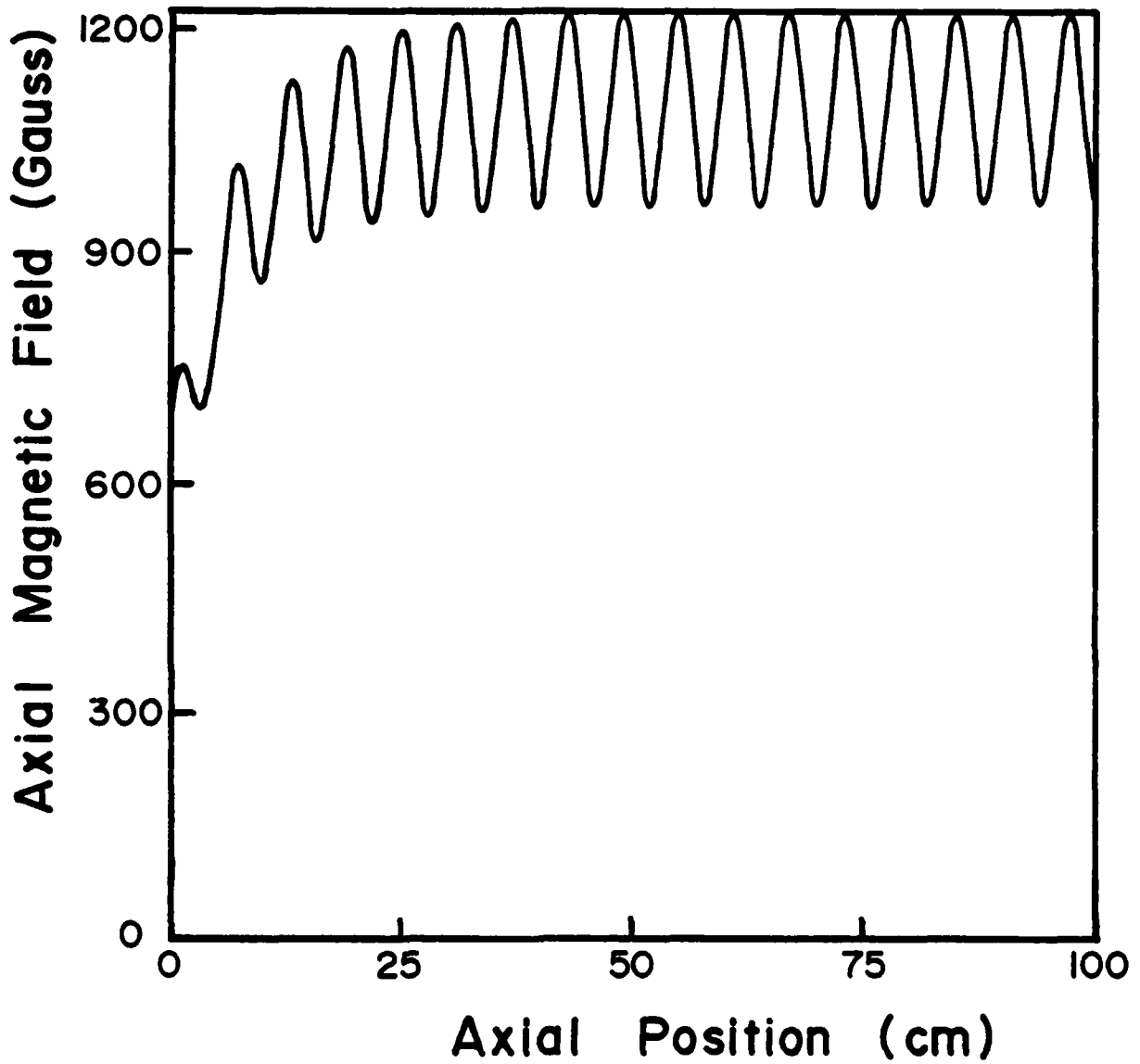


Figure 12. Plot of $B_z(r=0)$ vs. z in the diffusive wiggler. Face of solenoid is at $z = 0$.

axial field. However, the perpendicular component of the wiggler vanishes along the axis of the diffusive wiggler, so that only electrons that are significantly off axis can participate in the type of FEL interaction described previously. It has been pointed out, however, that an interaction that relies on the transverse energy in the beam can be exploited to obtain radiation from such a wiggler. This device has been called the Lowbitron (McMullin and Bekefi, 1981). The radiation frequency is approximately

$$\omega = (1 + \beta_z^2)^{1/2} \gamma_z^2 (v_z k_w + \Omega_0/\gamma). \quad (39)$$

This radiation is a result of electrons interacting with the axial component of the wiggler field. The Lowbitron interaction requires $k_w c \beta_{\perp} \gamma / \Omega_0 \ll 1$. The electron gyroradius must be sufficiently small that the transverse field modulation felt by the electron can be neglected compared with the longitudinal modulation.

VII. Radiation Measurements

We have carried out a series of measurements on the radiation using a diffusive wiggler. Radiation measurements have primarily consisted of a) spectral analysis using cylindrical cut-off filters and/or a gas breakdown spectrometer and b) approximate power measurements using either pressure thresholds for gas breakdown or calibrated crystal detectors and attenuators. Careful consideration has been given to the identification of the interaction modes, both cyclotron and FEL, and scaling measurements have been performed to verify these modes.

A. Gas Breakdown Spectrometer

The radiated power can be estimated from the pressure at which gas breakdown occurs. An empirical formula for the rms breakdown electric field E_b is

$$E_b = AP[1 + (a/P\lambda)^2]^{1/2}, \quad (40)$$

where $A = 3000 \text{ Vm}^{-1}\text{Torr}^{-1}$ and $a = 0.9 \text{ Torr-m}$ for air or nitrogen, P is the gas pressure in Torr, and λ is the wavelength in meters. Equation (40) has been checked against McDonald's gas breakdown data (McDonald, 1966) and agrees in the worst case to within 30%. This formula is valid on the high pressure side of the breakdown curve and for $\lambda < 30 \text{ cm}$, pulse lengths $> 1 \mu\text{s}$, low repetition rate ($< 100 \text{ pps}$), and electron diffusion lengths small compared to the chamber dimensions.

If the radiation is reflected from a boundary, a standing wave is set up with an amplitude given by

$$E^2 = E_1^2 (1 + \Gamma^2 - 2\Gamma \cos [2 \vec{k} \cdot \vec{x}]) \quad (41)$$

where E_1 is the magnitude of the incident wave, Γ the reflection coefficient, and k the wavenumber. The distance d between the peaks in the standing wave is determined by setting $2 \vec{k} \cdot \vec{x} = 2\pi$, so that

$$d = \frac{\lambda}{2 \cos \theta} \quad (42)$$

where λ is the wavelength of the radiation and θ the angle of incidence with respect to the surface normal. By adjusting the gas pressure so that the standing wave field amplitude is slightly higher than the breakdown field, localized gas breakdown will occur at the standing wave peaks. Then λ can be determined by measuring the distance between adjacent breakdown spots, and the power can be estimated from the pressure required to initiate observable breakdown.

Figure 13 shows a schematic of the spectrometer. Radiation is collected in the horn on the left. It then travels through a high pass filter and expands through the horn on the right to a collimating or weakly focusing lens. The microwaves are reflected from a metallic boundary located inside the gas filled chamber.

Figure 14 is a time integrated photograph of the resulting interference pattern. Microwave radiation has entered from the left of the photograph where the lens is located (but cannot be seen) and is reflected off a copper plate located at the right of the photograph (outlined by a light ring). All the white spots are due to light produced when the gas breaks down. Type 57 (ASA 3000) Polaroid film was used with a Graphflex camera (f/4.5) to obtain these results. The gas density was selected so that enough light was available for photographing the spots, but was kept low enough to prevent microwave reflections from the plasma. Thus for the measured pressure (25 Torr) and wavelength (4.5 cm), the electric field is determined from Eq. 40 to be about 1 kV/cm. From the spot diameter of 2.5 cm, the power is estimated for a plane wave to be 8 kW.

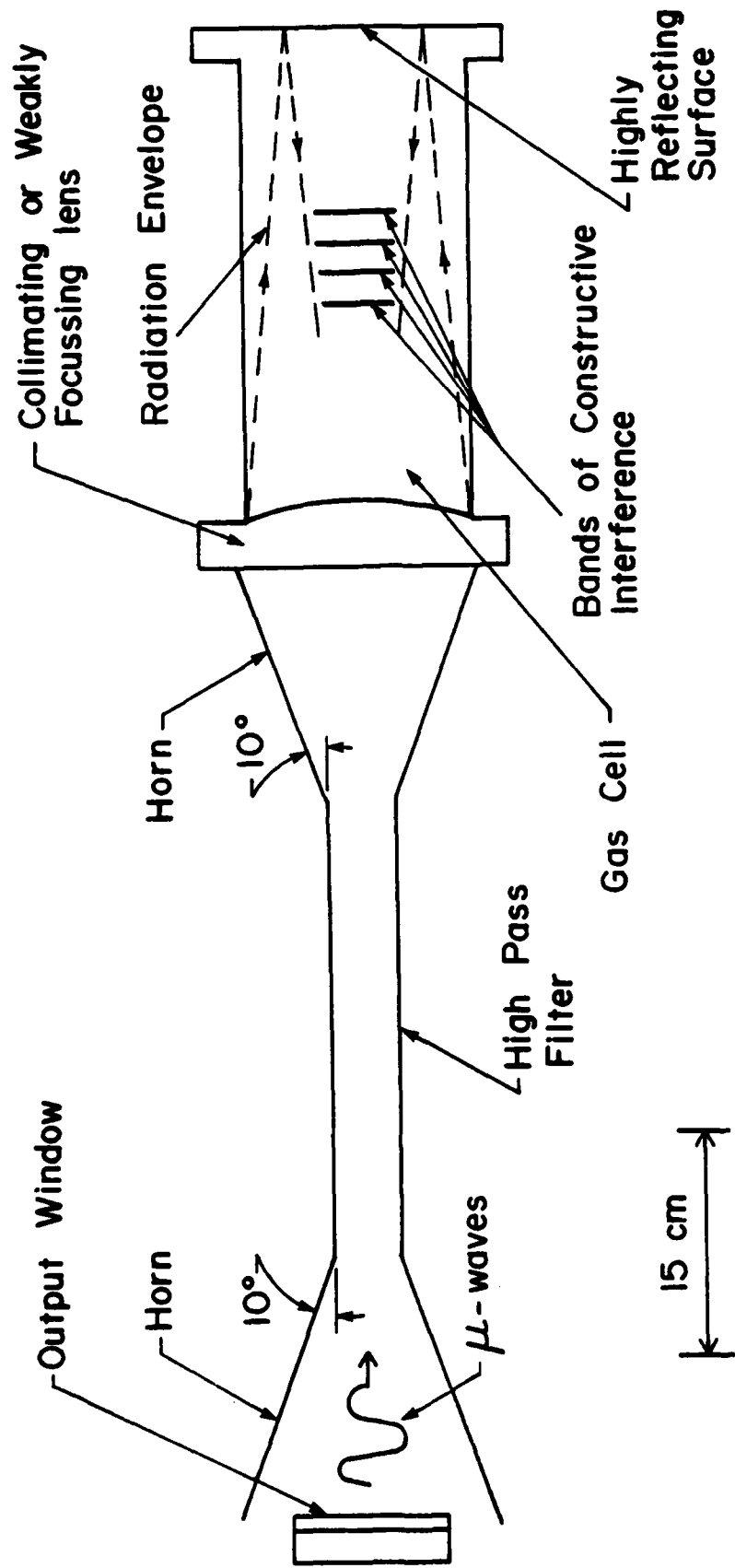


Figure 13. Schematic of gas breakdown spectrometer.

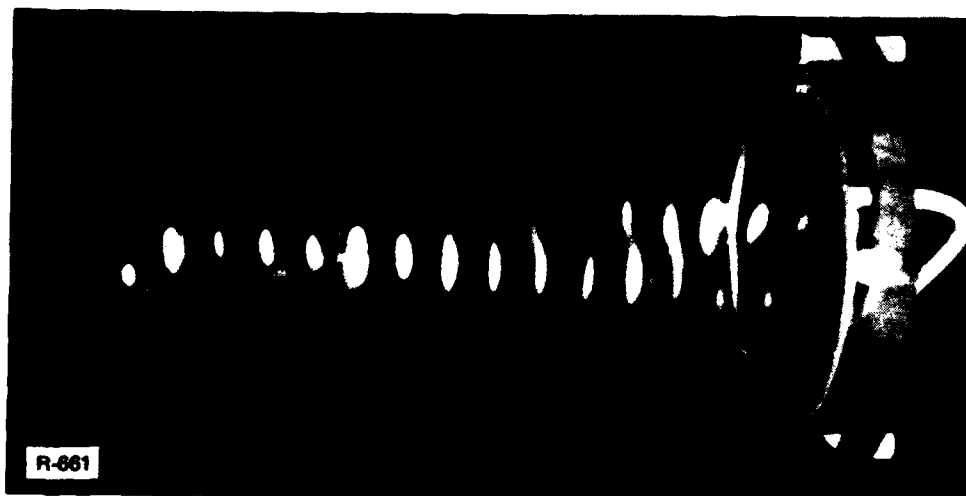


Figure 14. Open-shutter photograph of gas breakdown in 25 Torr nitrogen.
From the 2.25 cm spot spacing, the radiation wavelength is 4.5 cm.

This technique underestimates the power because there is considerable energy outside the radius of the observed spot. For example, in the case above the spot diameter is nearly a factor of 2 smaller than the wavelength, so clearly the radiation envelope is larger than the measured spot size.

We have identified this radiation as a TE_{01} mode that is excited at the 2nd harmonic of the electron cyclotron beam interaction. With similar measurements we have observed more than 100 kW of power at a wavelength of 7.5 cm. This mode was identified as a TE_{11} mode excited at the fundamental cyclotron beam interaction. The electron beam current in these experiments was 130 A, the voltage 550 keV for 2 μ sec, and the wiggler period was 6 cm. The gas breakdown spectrometer has been described in more detail elsewhere (Mako et al., 1982).

B. Mode Analysis and Experimental Results

The strongest interactions are expected when the phase velocities of the beam modes and waveguide modes are equal. The dispersion relation for the waveguide mode is

$$\omega^2 = \omega_{co}^2 + k^2 c^2 \quad (43)$$

where ω_{co} is the cutoff frequency. The dispersion relation for the free electron laser is

$$\omega = (k + k_w) v_z - \omega_p / \gamma^{3/2} \quad (44)$$

The last term is small at the current densities of this experiment and is neglected. The cyclotron mode dispersion relation is given by

$$\omega = k v_z + n \Omega_o / \gamma, \quad (45)$$

where $\Omega_o = eB_o/m$ and γ have been explicitly written to make the energy scaling clear.

Then the intersections of the FEL and cyclotron modes with a waveguide mode are found from Eqs. 43-45 to be

$$\omega_{\text{FEL}} = k_w v_z \gamma_z^2 \left[1 \pm \beta_z \sqrt{1 - \left(\frac{\omega_{\text{co}}}{k_w \gamma_z v_z} \right)^2} \right] \quad (46)$$

$$\omega_{\text{cyc}} = \frac{n \Omega_o \gamma_z^2}{\gamma} \left[1 \pm \beta_z \sqrt{1 - \left(\frac{\omega_{\text{co}} \gamma}{n \Omega_o \gamma_z} \right)^2} \right] \quad (47)$$

where $\omega_{\text{co}} = 2\pi c/a X_{nm}$, a is the waveguide radius and $X_{nm} = 3.41$ for TE_{11} , 2.61 for TM_{01} , 2.06 for TE_{21} , 1.14 for TM_{11} and 1.14 for TM_{02} modes.

A sketch of three dispersion relations is shown in Fig. 15. The cyclotron mode will be above the FEL mode if $n \Omega_o / \gamma > k_w v_z$. There are typically both high frequency and low frequency intersections of the FEL and cyclotron modes with the waveguide mode. However, the high frequency FEL intersection is the one which results in the usual FEL interaction. Also, the gyrotron typically operates at the low frequency cyclotron intersection, but a cyclotron

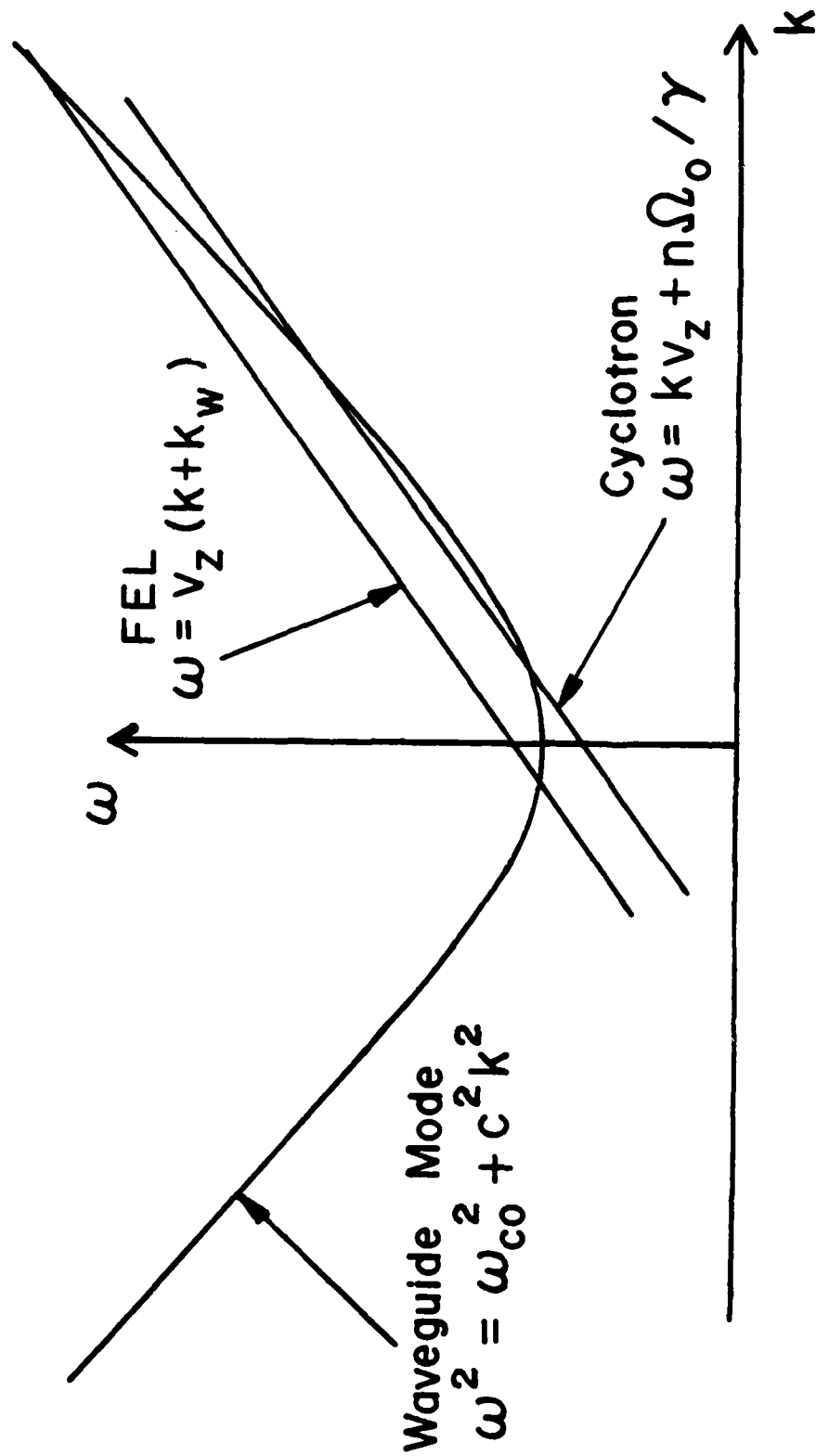


Figure 15. Dispersion curves showing a waveguide mode and the cyclotron and FEL beam lines. Radiation growth is expected at the intersection points, which are given by Eqs. 46 and 47.

interaction is also possible at the high frequency intersection. Figure 16 is a plot of the waveguide beam mode interactions that are possible for the parameters of the experiment. Both the first and second harmonics of the electron cyclotron interaction are shown, assuming $\gamma_z = 1.6$. The justification for this assumption will be given below. The arrows in the figure indicate the frequencies at which the strongest interactions were observed experimentally.

To positively identify the FEL mode at $f \approx 16$ GHz, we have varied the magnetic field and wiggler wavelength. It turns out that the cyclotron mode is very insensitive to B_0 in our parameter range. Because the magnetic moment is approximately conserved, the leading term for the cyclotron wave $\Omega_0 \gamma_z^2$ is nearly a constant for small changes in the magnetic field. Thus, the frequencies of the electron cyclotron modes increase only slightly with increasing magnetic field. However, the FEL frequency increases with a decreasing magnetic field because γ_z^2 varies as the inverse of B_0 .

Figure 17 contains the results of the mode identification experiments. The measurements were made using high pass cutoff filters, so each bar is an indication of the resolution. This technique integrates the total power above the cut off frequency of the particular filter. Thus, the power in a particular band is just the power measured with that filter minus the power measured with the next smaller diameter filter.

The arrow is the calculated FEL frequency with $\gamma_z = 1.6$. At $\lambda_w = 7$ cm and $B_0 = 2.45$ kG the calculated frequency is 11.6 GHz and this is where we see a factor of two increase in the signal amplitude. When the magnetic field

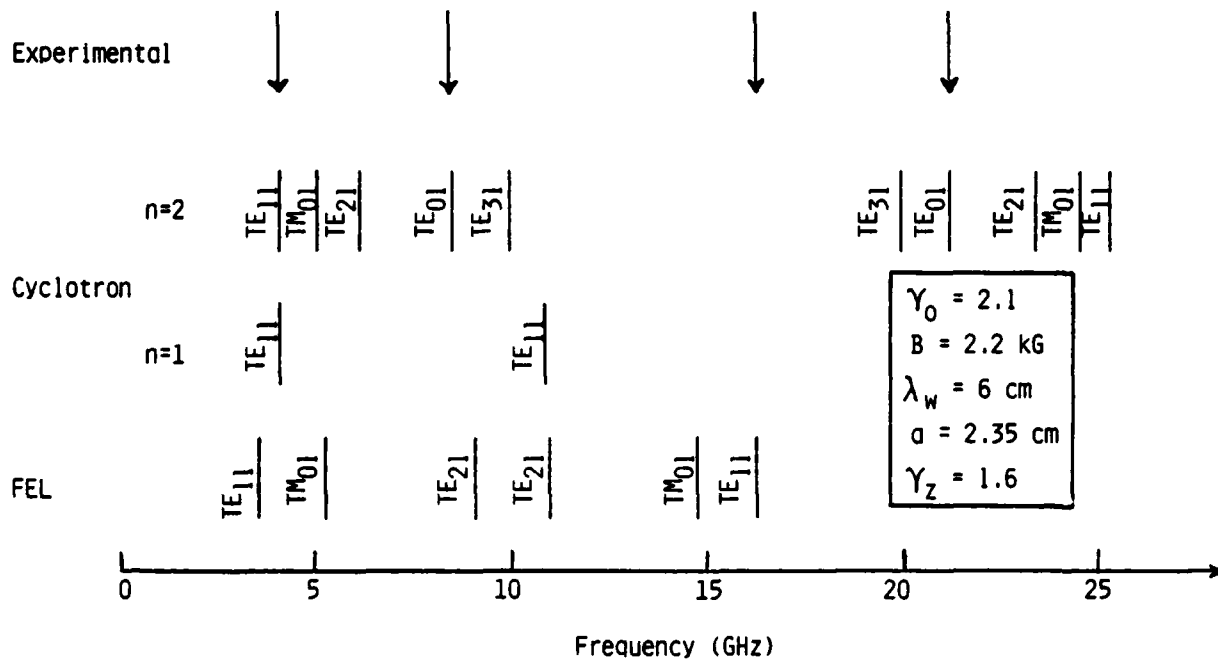


Figure 16. Beam-waveguide mode interactions which are possible with the experimental parameters. The arrows denote the measured output frequencies.

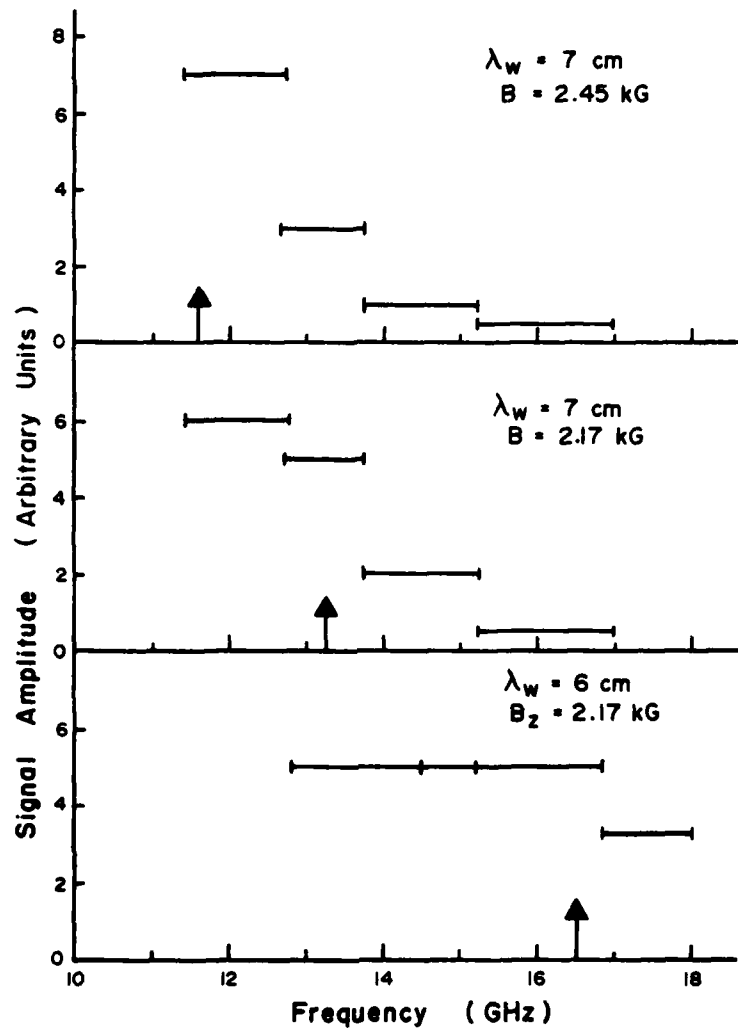


Figure 17. Frequency scaling of one particular mode with magnetic field and wiggler period, as determined by using a series of high-pass cut-off filters. Except as limited by the detector bandwidth, the signal amplitude shown in each frequency interval is proportional to the integrated power at all frequencies above the cut-off of the corresponding filter. Thus, power in a particular interval is indicated by a decrease in signal amplitude at the next higher interval. The arrows locate the theoretical frequency of the TE_{11} FEL mode, which agrees well with the observed spectra.

is reduced to 2.17 kG, the FEL frequency should increase to 13.2 GHz, and we observe a factor of two increase in that cutoff filter. At $\lambda_w = 6$ cm and $B_0 = 2.17$ kG, the FEL interaction should occur at 16.5 GHz and we observe a factor of 10 increase in that cutoff filter. We have also observed that the electron cyclotron mode at 21 GHz increases with magnetic field. We have looked for radiation from the Lowbitron interaction at $\omega \approx 2\gamma_z^2 (\Omega_0/\gamma + k_w v_z)$. This interaction requires perpendicular velocity and interacts with variations in the z component of the wiggler field. We did not see Lowbitron radiation that was comparable in amplitude with the FEL and 2nd harmonic cyclotron radiation.

In summary, we have observed free electron laser radiation from the long pulse induction linac. The FEL was operated in the superradiant mode. The power radiated in the FEL mode was approximately 10 kW with the beam interacting with the TE_{11} waveguide mode. Second harmonic electron cyclotron radiation of comparable amplitude was observed in the TE_{01} mode. Most of the power resulted from the low frequency cyclotron interaction. More than 100 kW of radiated power at the fundamental electron cyclotron mode was observed in the TE_{11} mode. In all cases the duration of the radiation was 2 μ sec. The thermal spread of the beam in the region requires FEL operation in the kinetic Compton regime.

The radiation spectrum is very sensitive to the average value of γ_z , which was determined by fitting the observed spectrum with interaction frequencies calculated using an assumed value of $\langle \gamma_z \rangle$. Then small variations in the magnetic and wiggler period were made to determine if the mode was an FEL or cyclotron mode. In this manner we were able to determine that $\langle \gamma_z \rangle$ had to be $1.6 \pm .2$.

Another way of estimating γ_z is by measuring the beam radius in the uniform field of the solenoid. Since the cathode in this experiment is in a magnetic field free region, the canonical angular momentum P_θ is zero. Then

$$\gamma m r v_\theta = e r A_\theta, \quad (48)$$

where A_θ is the magnetic vector potential which for a uniform magnetic field is $A_\theta = r B_z/2$. Then

$$\beta_\theta = \frac{1}{2} \frac{e B_z r}{\gamma m c}. \quad (49)$$

Experimentally, the rms beam radius was measured from time averaged x-ray scintillation pictures to be 1.3 cm when $B_z = 2.17$ kG and $\gamma = 2.1$. Thus conservation of P_θ alone gives $\beta_\perp = 0.4$ at this rms beam radius. Then

$$\gamma_z = \gamma / (1 + \beta_\perp^2 \gamma^2)^{1/2} = 1.6 \quad (50)$$

In addition, computer simulations of the induction linac free electron laser configuration have been carried out (Thompson et. al., 1982). The mean value of γ_z from the simulations was 1.61. Most of the energy spread comes at the transition between the induction linac transport system and the solenoidal field. Figure 18 is a plot of the induction linac FEL magnetic field profile. The diode is in a field free region at $z = 0$ and the last focusing coil of the linac is at 350 cm. The edge of the solenoid is at approximately 375 cm. The 2 kG magnetic field is required for a beam equilibrium radius that is consistent with a practical wiggler diameter.

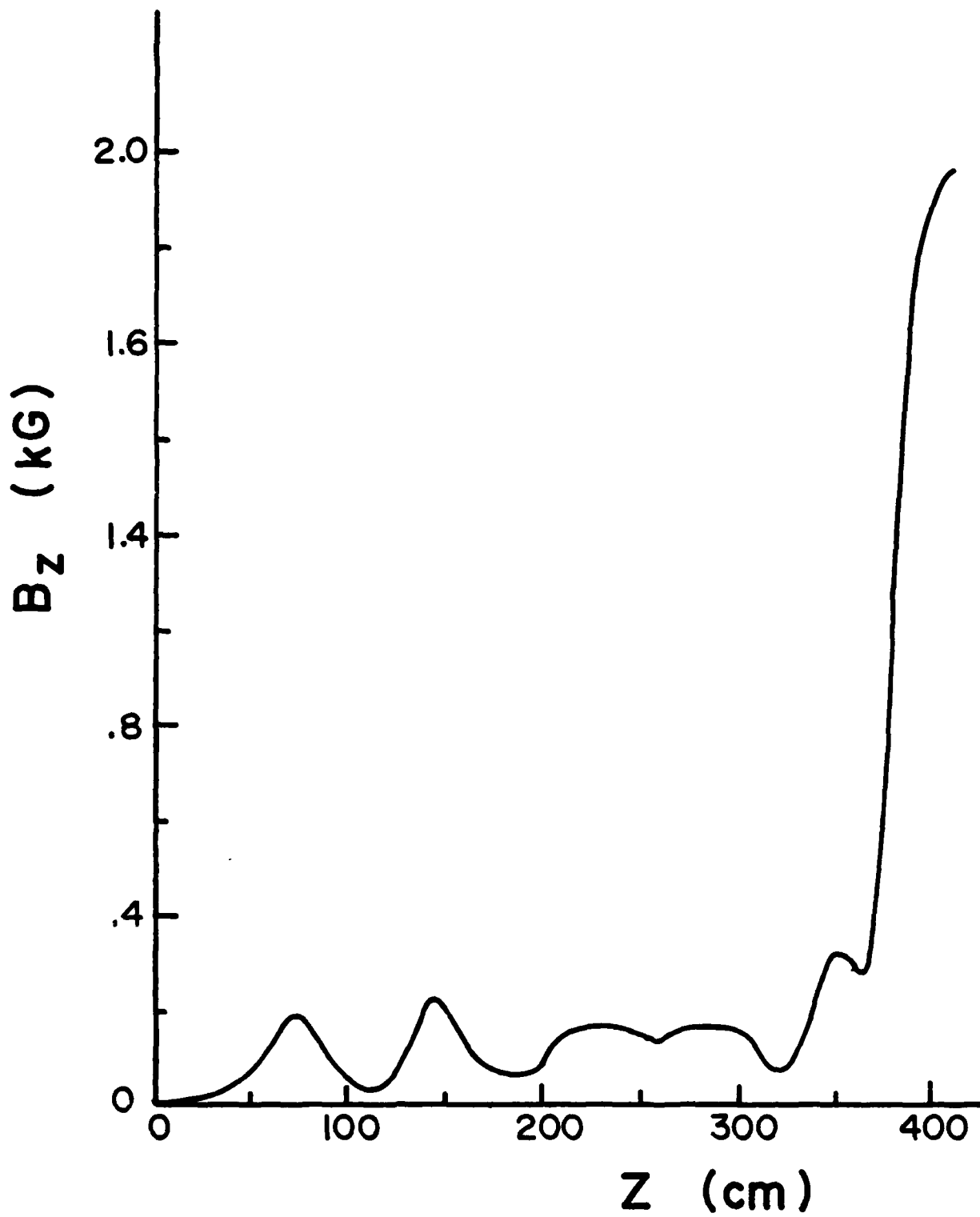


Figure 18. Axial magnetic field profile in the Long Pulse Induction Linac. Cathode is located at $z=0$ and the FEL solenoid begins at $z = 380$

Figure 19 is a plot of results from a static computer simulation of the beam transport from the cathode into the solenoid. The last accelerating gap of the induction module is not energized, so $\gamma = 2.1$ as the beam enters the last focusing coil. When the beam has reached the uniform field region $\langle \gamma_z \rangle$ is 1.6.

This problem of beam transport and matching represents one of the major design concerns for high current free electron lasers. The equilibrium of high current beams is sensitive to self electric and magnetic fields of the beam. Abrupt changes in the wall diameter or magnetic field profile induces betatron, or zero frequency cyclotron oscillations at $\omega = 0 = k\beta c - \Omega_0/\gamma$, so the period is $\lambda = 2\pi\beta c\gamma/\Omega_0$.

A spread in β across the beam radius will cause these oscillations to phase mix after a few periods. The perturbation then appears as an effective temperature.

In the present simulation the initial normalized emittance was $\epsilon_n = 180 \pi$ mrad-cm, whereas the effective final emittance was $\epsilon_n = \gamma r \beta_{l \text{ rms}} = 940 \pi$ mrad-cm. Almost all of this increase in emittance came in the transition to the solenoid. This is why the final emittance for the hot and cold cathode is about the same. These problems can and have been avoided in Marx-pulse line beam generators by immersing the diode in a very strong magnetic field. This minimizes the radial excursion and effective emittance growth. This approach becomes difficult when long pulse times are required and one must use large area hot cathodes to get kiloampere electron beams. One can conclude from this that the design of the beam transport system for an induction linac FEL is at least as important as the diode design.

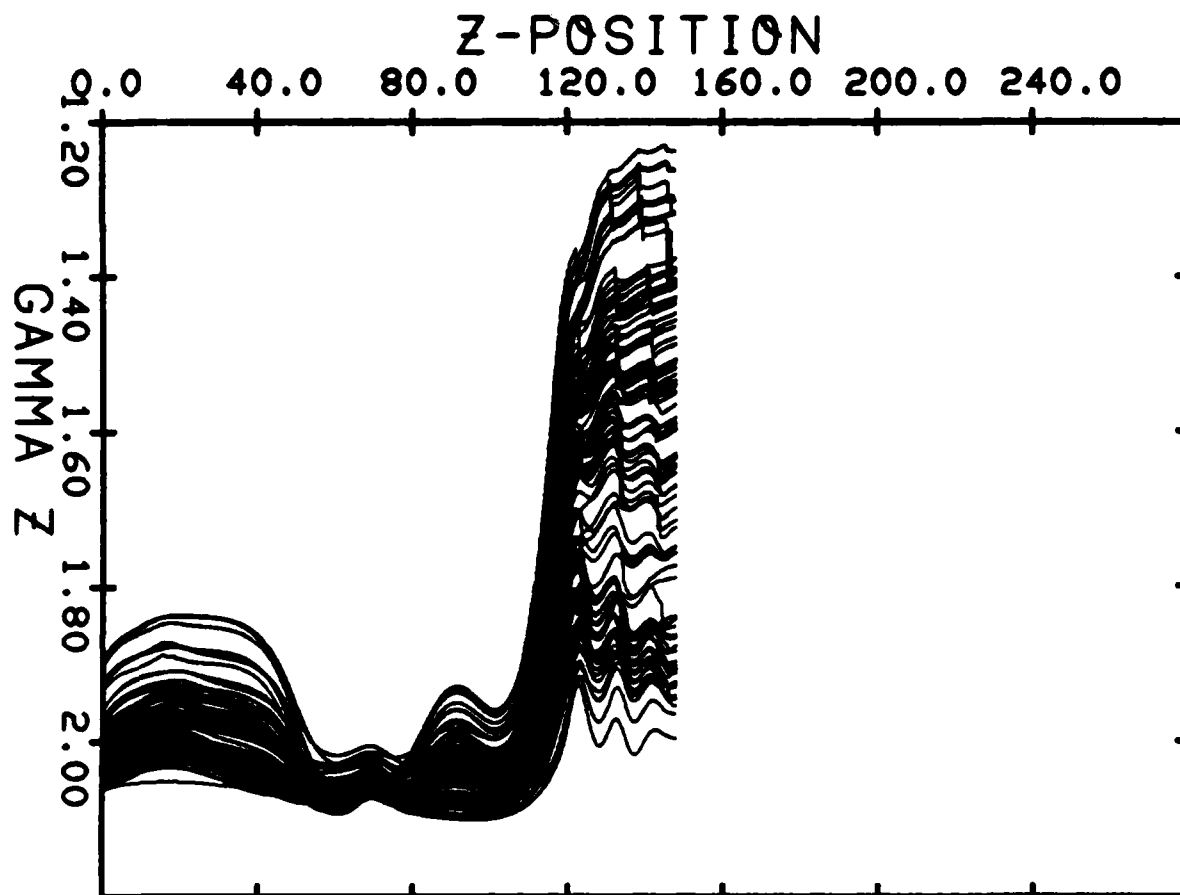


Figure 19. Variation of γ_z with z for electrons in a computer simulation of the experiment. The large spread in γ_z occurs as the beam enters the solenoidal field.

VIII. Conclusions and Future Directions

Improvements in the beam transport are clearly needed to operate in the Raman regime. One of the advantages of operating in the cold beam limit is that the efficiency of the FEL is higher and can be enhanced by tapering the wiggler period. Once the beam is trapped in the pondermotive wave, the phase velocity of the wave can be reduced gradually to extract energy from the beam. Figure 20 is a plot of efficiency vs distance for an untapered and tapered wiggler. These results are from a computer simulation of the present experiment. Whereas the intrinsic efficiency is about 5 percent, the tapered wiggler efficiency is in excess of 20 percent.

To go to shorter wavelengths the FEL can be operated as a two stage device. The output from stage one at $\lambda_1 = \lambda_w / 2\gamma^2$ can be used as the output for the second stage to give

$$\lambda_2 = \frac{\lambda_1}{4\gamma^2} = \frac{\lambda_w}{8\gamma^4} . \quad (51)$$

To obtain a high voltage high current accelerator and achieve a high gain, high power short wavelength FEL, the long pulse induction module can be converted into a racetrack accelerator (Roberson, 1981; Mondelli and Roberson, 1982). This takes advantage of the long pulse to give a voltage

$$V = V_g T / \tau \quad (52)$$

where V_g is the voltage gain of the module, T the time the module is on, and τ the time it takes the beam to go around the racetrack. In the present case a 30 nsec path length would result in a 26 MeV beam with the $2 \mu\text{s}$, 0.4 MV module.

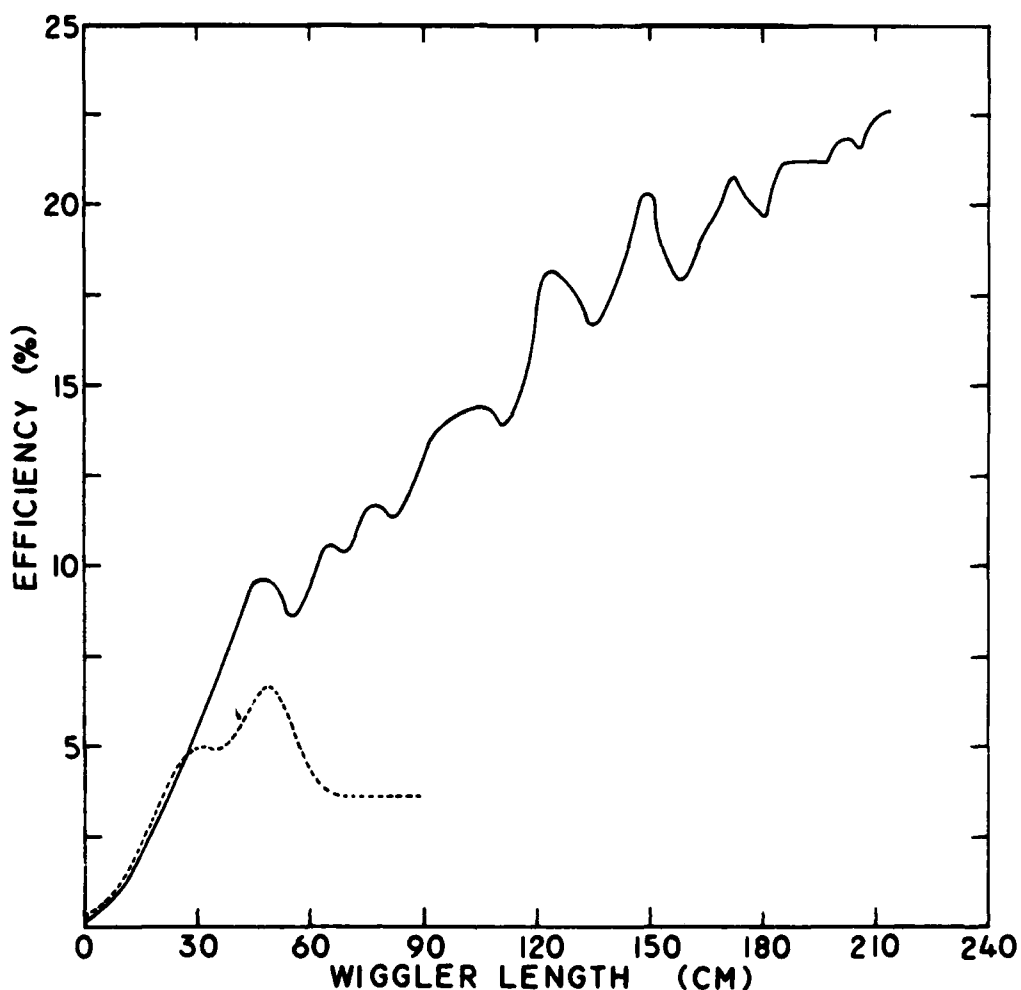


Figure 20. Theoretical FEL efficiency vs. interaction length with and without a tapered wiggler. The parameters used for the calculation are those of the experiment.

Acknowledgements

We would like to thank A. Mondelli and S. Slinker for their contributions on the diffusive wiggler and beam transport; H. Freund for discussion on the linear wiggler; C.M. Tang for simulations of the linear wiggler; J.R. Thompson and B. Moore for computer simulations of the beam transport and Mark Wilson for his help in setting up the induction linac at NRL.

References

Barbini, R. and Vignola, G. (1982). In "Physics of Quantum Electronics" (S. Jacobs, H. Pilloff, M. Scully, G. Moore, M. Sargent III, and R. Spitzer, eds.), Vol. 8, pp. 235-262. Addison-Wesley, Reading, MA.

Bazin, C., Billardon, M., Deacon, D.A.G., Ellaume, P., Farge, Y., Madey, J.M.J., Ortega, J.M., Petroff, Y., Robinson, K.E., and Velghe, M. (1982). In "Physics of Quantum Electronics" (S. Jacobs, H. Pilloff, M. Scully, G. Moore, M. Sargent III, and R. Spitzer, eds.), Vol. 8, pp. 89-118. Addison-Wesley, Reading, MA.

Bizzarri, U., Ciocci, F., Dattoli, G., DeAngelis, A., Fiorentino, E., Gallerano, G.P., Marino, A., Renieri, A., and Vignati, A., (1982). In "Physics of Quantum Electronics" (S. Jacobs, H. Pilloff, M. Scully, G. Moore, M. Sargent III, and R. Spitzer, eds.), Vol. 9, pp. 677-696. Addison-Wesley, Reading, MA.

Blewett, J.P. and Chasman, R. (1977), "Journ. of Appl. Phys. 48, 2692.

Boehmer, H., Caponi, M.Z., Edighoffer, J., Fornaca, S., Munch, J., Neil, G.R., Saur, B., and Shih, C. (1982). Phys. Rev. Lett. 48, 141.

Deacon, D.A.G., Elias, L.R., Madey, J.M.J., Ramian, G.J., Schwettman, H.A., and Smith, T.I. (1977). Phys. Rev. Lett. 38, 892.

Efthimion, P.C. and Schlesinger, S.P. (1977). Phys. Rev. A. 16, 633.

Elias, L.R., Fairbanks, W.M., Madey, J.M.J., Schwettman, H.A., and Smith, T.I. (1976). Phys. Rev. Lett. 36, 717.

Elias, L.R. and Ramian, G. (1982). In "Physics of Quantum Electronics", (S. Jacobs, H. Pilloff, M. Scully, G. Moore, M. Sargent III, and R. Spitzer, eds.), Vol. 9, pp. 577-602. Addison-Wesley, Reading, MA.

Friedman, M. and Herndon, M. (1972). Phys. Rev. Lett. 28, 210.

Gaupp, A. (1982). In "Physics of Quantum Electronics", (S. Jacobs, H. Pilloff, M. Scully, G. Moore, M. Sargent III, and R. Spitzer, eds.), Vol. 8, pp. 263-274. Addison-Wesley, Reading, MA.

Gilgenbach, R.M., Marshall, T.C., and Schlesinger, S.P. (1979) Phys. Fluids 22 971-977.

Granatstein, V.L., Herndon, M., Parker, R.K., and Schlesinger, S.P. (1974). IEEE Trans. Microwave Theory Tech. 22, 1000.

Granatstein, V.L., Schlesinger, S.P., Herndon, M., Parker, R.K., and Pasour, J.A. (1977). Appl. Phys. Lett. 30, 384.

Granatstein, V.L., ed. (1981). "Special Issue on Gyrotrons." Int. J. Electronics 51, 275-606.

Grossman, A., Marshall, T.C., and Schlesinger, S.P. (1983) Phys. Fluids 26,

Hasegawa, A. (1978) Bell Syst. Tech. J. 57, 3069.

Jacobs, K.D., Shefer, R.E., and Bekefi, G. (1980). Appl. Phys. Lett. 37, 583.

Kroll, N.A. and McMullin, W.A. (1978). Phys. Rev. A 17, 300-308.

Kulke, B., Ravenscroft, D.S., and Vogtlin, G.E. (1982), IEEE Trans. Nucl. Sci. NS-28, 2882.

Leiss, J.E., Norris, N.J. and Wilson, M.A., (1980), Particle Accelerators 10 , 223.

Luccio, A. (1982). In "Physics of Quantum Electronics" (S. Jacobs, H. Pilloff, M. Scully, G. Moore, M. Sargent III, and R. Spitzer, eds.), Vol. 8, pp. 153-180. Addison-Wesley, Reading, MA.

Mako, F., Pasour, J.A., Roberson, C.W., and Lucey, R. (1982). NRL Memo Report #4945.

Marshall, T.C., Talmadge, S., and Efthimion, P. (1977a). Appl. Phys. Lett. 31, 302.

Marshall, T.C., Sandel, F.L., and Gilgenbach, R.M., (1977b). Proc. Sec. Int. Topical Conf. on High Power Electron and Ion Beam Res. Technol., pp. 697-702.

McDermott, D.B., Marshall, T.C., Schlesinger, S.P., Parker, R.K., and Granatstein, V.L. (1978). Phys. Rev. Lett. 41, 1368-1371.

McDonald, A.D., (1966) "Microwave Breakdown in Gases", John Wiley & Sons.

Mondelli, A. and Roberson, C.W. "Energy Scaling Laws for the Racetrack Induction Accelerator", NRL Memo Report

Mross, M.R., Marshall, T.C., Efthimion, P., and Schlesinger, S.P. (1976). Digest Sec. Int. Conf. Winter School on Submillimeter Waves and Appl. (IEEE Cat. No. 76 CH 1152-8 MTT), pp. 128-129.

Nation, J.A. (1970). Appl. Phys. Lett. 17, 491.

Neil, V.K. (1979). Jason Technical Report JSR-79-10, SRI International, Arlington, VA.

Parker, R.K., Jackson, R.H., Gold, S.H., Freund, H.P., Granatstein, V.L., Efthimion, P.C., Herndon, M. and Kinkead, A.K. (1982) Phys. Rev. Lett. 48, 238.

Pasour, J.A., Roberson, C.W., and Mako, F. (1982) J. Appl. Phys. 53,

Phillips, R.M. (1960). IRE Trans. on Electron Dev. 7, 231.

Prohaska, R., and Fisher, A. (1982). Rev. Sci. Instrum. 53, 1092.

Prosnitz, D. and Sessler, A.M. (1982). In "Physics of Quantum Electronics" (S. Jacobs, H. Pilloff, M. Scully, G. Moore, M. Sargent III, and R. Spitzer, eds.), Vol. 9, pp. 651-670, Addison-Wesley, Reading, MA.

Ramirez, J.J. and Cook, D.L. (1980). J. Appl. Phys. 51, 4602.

Roberson, C.W. (1981), IEEE Trans. Nucl. Sci. NS-28, 3433.

Roberson, C.W., Pasour, J.A., Kapetanacos, C.A., Sprangle, P., Golden, J., Mako, F., and Lucey, R. (1982). In "Physics of Quantum Electronics" (S. Jacobs, H. Pilloff, M. Scully, G. Moore, M. Sargent III, and R. Spitzer, eds.), Vol. 9, pp. 727-740. Addison-Wesley, Reading, MA.

Shaw, E.D. and Patel, C.K.N. (1982). In "Physics of Quantum Electronics" (S. Jacobs, H. Pilloff, M. Scully, G. Moore, M. Sargent III, and R. Spitzer, eds.), Vol. 9, pp. 671-676. Addison-Wesley, Reading, MA.

Shefer, R.E. and Bekefi, G. (1982). In "Physics of Quantum Electronics" (S. Jacobs, H. Pilloff, M. Scully, G. Moore, M. Sargent III, and R. Spitzer, eds.), Vol. 9., pp. 703-726, Addison-Wesley, Reading, MA.

Sloan, M.L. and Davis, H.A. "Design and Testing of Low Temperature Intense Electron Beam Diodes" Accepted for publication in Physics of Fluids.

Sprangle, P., Smith, R.A., and Granatstein, V.L., (1979). In "Infrared and Millimeter Waves" (K.J. Button, ed.) Vol. 1, pp. 279-327. Academic Press, New York.

Sprangle, P. and Manheimer, W.M. (1975). Phys. of Fluids 18, 224.

Sprangle, P., Granatstein, V.L., and Baker, L. (1975). Phys. Rev. A 12, 1697.

Thompson, J.R. Moore, B.N., Sloan, M.L. and Uglum, J.R. (1982). Bull. Am. Phys. Soc. 27, 1011.

Warren, R.W., Brau, C.A., Newnam, B.E., Stein, W.E., Winston, J.G., and Young, L.M. (1982). In "Physics of Quantum Electrons" (S. Jacobs, H. Pilloff, M. Scully, G. Moore, M. Sargent III, and R. Spitzer, eds.), Vol. 8, pp. 397-414. Addison-Wesley, Reading, MA.

END

FILMED

3-83

DTIC